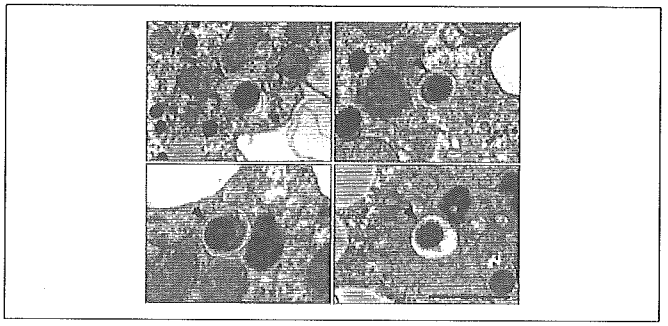

FIGURE 5. **Excess peroxisomes are surrounded by autophagosome.** $Atg7^{F/+}$:Mx1 mice were treated with DEHP for 2 weeks and then injected with leupeptin as described under "Experimental Procedures." The mice were sacrificed, and the livers were dissected out and processed for electron microscopic examination. These images show representative autophagosomes surrounding peroxisomes. Four typical electron micrographs are represented. *Arrowheads* indicate the engulfment of peroxisome(s) by isolated membranes. *Bars*, 1 μm.

lysosomal cysteine proteinase inhibitor, into a 2-week DEHP-treated control $Atg7^{F/+}$:Mx1 mouse resulted in marked accumulation of autophagosomes, and some peroxisomes were surrounded by a double-membrane structure, autophagosome, in control hepatocytes (Fig. 5). No autophagosome was identified in hepatocytes of $Atg7^{F/F}$:Mx1 mice (data not shown). These lines of evidence indicated that the autophagic machinery mediated is essential for selective clearance of excess peroxisomes, as it is so for starvation-induced autophagy in the mouse liver.

DISCUSSION

Most cellular components, if not all, are regulated quantitatively to maintain cell homeostasis. For this regulation, there are growing lines of evidence for the importance of the balance between biosynthesis and degradation. Peroxisomes, a typical cellular component, are dynamic organelles induced and degraded in response to extracellular cues (8). However, little is known about the mechanism for peroxisome degradation in mammals. There are two major concepts for degradation of peroxisomes, *i.e.* autophagic machinery and autolysis (34, 35). By the analysis of autophagy-deficient livers, we showed the first direct evidence that peroxisomal breakdown is mainly, if not entirely, dependent on autophagic machinery. Based on quantitative densitometry with two peroxisome marker enzymes (Fig. 2, PT and BF) as well as morphometry of the electron micrographs (Fig. 4), ~70–80% of peroxisomes induced by DEHP were degraded via autophagy during 1 week after discontinuation of the drug administration.

Considering peroxisome degradation by autophagic machinery in mammals, it is important to know whether the process occurs via micropexophagy or macropexophagy. In methylotrophic yeast species, it is well established that the autophagy-related process, termed pexophagy, induces a rapid and selective degradation of excess peroxisomes (13). In *P. pastoris* cells, following a shift from methanol to ethanol or glucose, unnecessary peroxisomes are degraded by macropexophagy and micropexophagy, respectively (9). Macropexophagy is the degradation pathway in which autophagosomes selectively surround excess peroxisomes. On the other hand, in micropexophagy, the excess peroxisomes are not degraded through autophagosome formation. The initial step in micropexophagy is invagination and septation of a vacuole followed by engulfment of the peroxisomes by the vacuole. In the final stage, the edges of the vacuole fuse with each other followed by vacuolar degradation of the peroxisomal membrane and its contents. Because *ATG7* is essential for both macropexophagy and micropexophagy in *P. pastoris* cells, it is plausible that excess peroxisomes in mammalian cells are also degraded by both macroautophagy and micropexophagy. Our data using electron microscopy revealed that autophagosomes preferentially surrounded excess peroxisomes in control hepatocytes (Fig. 5), suggesting that DEHP-induced peroxisomes are degraded mainly through the process of macropexophagy. Thus, we could show the selective role of autophagic machinery in the clearance of surplus peroxisomes after induction of peroxisomes by phthalate esters.

Recent studies provided evidence for the involvement of the autophagic machinery in selective sequestration of proteins in the cell. For example, the precursor form of aminopeptidase I (prApe1) is a selective cargo molecule of autophagy in yeast (36), and cytosolic acetaldehyde dehydrogenase (Ald6p) is preferentially transported to vacuoles via autophagosomes in yeast (37). Consistently, the autophagic machinery could also selectively eliminate pathogenic group A *Streptococci* invading the cells (38). These reports strongly suggest that autophagosomes sequester the cytosolic protein(s) and invading pathogens in a highly selective manner. We recently reported that *Atg7*-deficient hepatocytes exhibit impaired constitutive autophagy responsible for selective degradation of ubiquitinated proteins (20). Our previous findings together with the present results suggest that the autophagic process eliminates abnormal and/or excess proteins and organelles including peroxisomes in a selective manner even under normal conditions. How the autophagy machinery recognizes these organelles to degrade them awaits further investigation.

Acknowledgment—We thank Tsuguka Kouno for technical assistance.

REFERENCES

1. Lazarow, P. B., and Fujiki, Y. (1985) *Annu. Rev. Cell Biol.* **1,** 489–530
2. Heiland, I., and Erdmann, R. (2005) *FEBS J.* **272,** 2362–2372
3. Reddy, J. K., Azarnoff, D. L., Hignite, C. E. (1980) *Nature* **283,** 397–398
4. Reddy, J. K., Lalwani, N. D. (1983) *CRC Crit. Rev. Toxicol.* **12,** 1–58
5. Nicholls-Grzemski, F. A., Calder, I. C., and Priestly, B. G. (1992) *Biochem. Pharmacol.* **7,** 1395–1396
6. Vanden Henvel, J. P. (1999) *Toxicol. Sci.* **47,** 1–8
7. Yokota, S. (1993) *Eur. J. Cell Biol.* **61,** 67–80
8. Subramani, S. (1998) *Physiol. Rev.* **78,** 171–188
9. Farre, J. C., and Subramani, S. (2004) *Trends Cell Biol.* **14,** 515–523
10. Kim, J., Kamada, Y., Stromhaug, P. E., Guan, J., Hefner-Gravink, A., Baba, M., Scott, S. V., Ohsumi, Y., Dunn, W. A., Jr., and Klionsky, D. J (2001) *J. Cell Biol.* **153,** 381–396
11. Stromhaug, P. E., Bevan, A., and Dunn, W. A., Jr. (2001) *J. Biol. Chem.* **276,** 42422–42435
12. Bellu, A. R., Komori, M., Klei, I. J., Kiel, J. A., and Veenhuis, M. (2001) *J. Biol. Chem.* **276,** 44570–44574
13. Bellu, A. R., and Kiel, J. A. (2003) *Microsc. Res. Tech.* **61,** 161–170
14. Ano, Y., Hattori, T., Oku, M., Mukaiyama, H., Baba, M., Ohsumi, Y., Kato, N., and Sakai, Y. (2005) *Mol. Biol. Cell* **16,** 446–457
15. Klionsky, D. J., and Ohsumi, Y. (1999) *Annu. Rev. Cell Dev. Biol.* **15,** 1–32
16. Kim, J., and Klionsky, D. J. (2000) *Annu. Rev. Biochem.* **69,** 303–342
17. Kissova, I., Deffieu, M., Manon, S., and Camougrand, N. (2004) *J. Biol. Chem.* **279,** 39068–39074
18. Lemasters, J. J. (2005) *Rejuvenation Res.* **8,** 3–5
19. Tanida, I., Mizushima, N., Kiyooka, M., Ohsumi, M., Ueno, T., Ohsumi, Y., and Kominami, E. (1999) *Mol. Biol. Cell* **10,** 1367–1379
20. Komatsu, M., Waguri, S., Ueno, T., Iwata, J., Murata, S., Tanida, I., Ezaki, J., Mizushima, N., Ohsumi, Y., Uchiyama, Y., Kominami, E., Tanaka, K., and Chiba, T. (2005) *J. Cell Biol.* **169,** 425–434
21. Kabeya, Y., Mizushima, N., Ueno, T., Yamamoto, A., Kirisako, T., Noda, T., Kominami, E., Ohsumi, Y., and Yoshimori, T. (2000) *EMBO J.* **19,** 5720–5728
22. Mizushima, N., Noda, T., Yoshimori, T., Tanaka, Y., Ishii, T., George, M. D., Klionsky, D. J., Ohsumi, M., and Ohsumi, Y. (1998) *Nature* **395,** 395–398
23. Ichimura, Y., Kirisako, T., Takao, T., Satomi, Y., Shimonishi, Y., Ishihara, N., Mizushima, N., Tanida, I., Kominami, E., Ohsumi, M., Noda, T., and Ohsumi, Y. (2000) *Nature* **408,** 488–492
24. Yuan, W., Stromhaug, P. E., and Dunn, W. A., Jr. (1999) *Mol. Biol. Cell* **10,** 1353–1366
25. Tanida, I., Tanida-Miyake, E., Ueno, T., and Kominami, E. (2001) *J. Biol. Chem.* **276,** 1701–1706

26. Tanida, I., Tanida-Miyake, E., Nishitani, T., Komatsu, M., Yamazaki, H., Ueno, T., and Kominami, E. (2002) *Biochem. Biophys. Res. Commun.* **292,** 256–262
27. Tanida, I., Tanida-Miyake, E., Komatsu, M., Ueno, T., and Kominami, E. (2002) *J. Biol. Chem.* **277,** 13739–13744
28. Asanuma, K., Tanida, I., Shirato, I., Ueno, T., Takahara, H., Nishitani, T., Kominami, E., and Tomino, Y. (2003) *FASEB J.* **17,** 1165–1167
29. Tanida, I., Minematsu-Ikeguchi, N., Ueno, T., and Kominami, E. (2005) *Autophagy* **1,** 84–91
30. de Duve, C., Pressman, B. C., Gianetto, R., Wattiaux, R., and Appelmans, F. (1955) *Biochem. J.* **60,** 604–617
31. Usuda, N., Yokota, S., Ichikawa, R., Hashimoto, T., and Nagata, T. (1991) *J. Histochem. Cytochem.* **39,** 95–102
32. Tsukamoto, T., Yokota, S., and Fujiki, Y. (1990) *J. Cell Biol.* **110,** 651–660
33. Ezaki, J., Wolfe, L. S., Higuti, T., Ishidoh, K., and Kominami, E. (1995) *J. Neurochem.* **64,** 733–741
34. Yokota, S., Oda, T., and Fahimi, H. D. (2001)) *J. Histochem. Cytochem.* **49,** 613–621
35. Yokota, S. (2003) *Microsc. Res. Tech.* **61,** 151–160
36. Shintani, T., and Klionsky, D. J. (2004) *J. Biol. Chem.* **279,** 29889–29894
37. Onodera, J., and Ohsumi, Y. (2004) *J. Biol. Chem.* **279,** 16071–16076
38. Nakagawa, I., Amano, A., Mizushima, N., Yamamoto, A., Yamaguchi, H., Kamimoto, T., Nara, A., Funao, J., Nakata, M., Tsuda, K., Hamada, S., and Yoshimori, T. (2004) *Science* **306,** 1037–1040

THE JOURNAL OF BIOLOGICAL CHEMISTRY
Vol. 280, No. 22, Issue of June 3, pp. 21515–21521, 2005
Printed in U.S.A.

Unsaturated Fatty Acids Induce Cytotoxic Aggregate Formation of Amyotrophic Lateral Sclerosis-linked Superoxide Dismutase 1 Mutants*

Received for publication, February 28, 2005
Published, JBC Papers in Press, March 29, 2005, DOI 10.1074/jbc.M502230200

Yeon-Jeong Kim‡, Reiko Nakatomi§, Takumi Akagi§, Tsutomu Hashikawa§, and Ryosuke Takahashi‡¶‖

From the Laboratories for ‡Motor System Neurodegeneration and §Neural Architecture, RIKEN Brain Science Institute, Saitama 351-0198, Japan and ¶Department of Neurology, Kyoto University Graduate School of Medicine, Kyoto 606-8507, Japan

Formation of misfolded protein aggregates is a remarkable hallmark of various neurodegenerative diseases including Alzheimer disease, Parkinson disease, Huntington disease, prion encephalopathies, and amyotrophic lateral sclerosis (ALS). Superoxide dismutase 1 (SOD1) immunoreactive inclusions have been found in the spinal cord of ALS animal models and patients, implicating the close involvement of SOD1 aggregates in ALS pathogenesis. Here we examined the molecular mechanism of aggregate formation of ALS-related SOD1 mutants *in vitro*. We found that long-chain unsaturated fatty acids (FAs) promoted aggregate formation of SOD1 mutants in both dose- and time-dependent manners. Metal-deficient SOD1s, wild-type, and mutants were highly oligomerized compared with holo-SOD1s by incubation in the presence of unsaturated FAs. Oligomerization of SOD1 is closely associated with its structural instability. Heat-treated holo-SOD1 mutants were readily oligomerized by the addition of unsaturated FAs, whereas wild-type SOD1 was not. The monounsaturated FA, oleic acid, directly bound to SOD1 and was characterized by a solid-phase FA binding assay using oleate-Sepharose. The FA binding characteristics were closely correlated with the oligomerization propensity of SOD1 proteins, which indicates that FA binding may change SOD1 conformation in a way that favors the formation of aggregates. High molecular mass aggregates of SOD1 induced by FAs have a granular morphology and show significant cytotoxicity. These findings suggest that SOD1 mutants gain FA binding abilities based on their structural instability and form cytotoxic granular aggregates.

Amyotrophic lateral sclerosis (ALS)[1] is a progressive and fatal neurodegenerative disorder that mainly affects motor neurons in the brain stem and spinal cord. Approximately 10% of ALS patients are familial cases, with autosomal dominant inheritance. More than 90 different mutations in the gene coding for superoxide dismutase 1 (SOD1) have been identified in about 20% of familial ALS (FALS) families (1, 2). Although the molecular mechanisms of selective motor neuron degeneration by SOD1 mutants in FALS remain largely unknown, common pathological features of conformational diseases, as evidenced by SOD1 immunoreactive inclusions, are found in the spinal cord of ALS patients and in the SOD1 mutant FALS mouse model (3–8). The characteristics of FALS resemble those of many other neurodegenerative diseases in which a causative protein undergoes a conformational rearrangement, which endows it with a tendency to aggregate and form deposits within affected tissues.

SOD1 is a 32-kDa homodimeric enzyme that decreases the intracellular concentration of superoxide radicals by catalyzing their dismutation to O_2 and H_2O_2. ALS-linked mutations of SOD1 are distributed throughout the primary and tertiary structures, and most mutations appear unrelated to the dismutase activity. Many biochemical and biophysical studies have reported that SOD1 mutants are structurally unstable compared with wild-type forms (10–13). These observations suggest that the mutations primarily affect the structural stability of SOD1 rather than the enzyme activity.

The half-life of SOD1 mutants is shorter than that of wild-type forms in cultured cells (14). SOD1 mutants form a complex with Hsp70 and CHIP, which promotes degradation of SOD1 through the ubiquitin-proteasome system (15). Hsp70 directly binds metal-deficient wild-type SOD1 as well as SOD1 mutants, suggesting that destabilized SOD1 is targeted by the molecular chaperone system (15, 16). These observations imply that structural stability of SOD1 may also be strongly involved in refolding by the chaperone or in degradation of SOD1 by the ubiquitin-proteasome system. On the other hand, aggregates of mutant SOD1 are observed to have aggresome-like morphology when cells are treated with a proteasome inhibitor (14). This aggresome-like morphology resembles pathological inclusions of neurodegenerative diseases in affected tissues. These findings suggest that in disease states, misfolded proteins overwhelm the protein handling systems, including chaperones and proteasomes. Therefore, the formation of cellular inclusions may be required for other factors to act as modulators to promote protein aggregates. In fact, lipid molecules, including unsaturated fatty acids (FAs), phosphatidylserine, and phosphatidylinositol, promote amyloidogenesis of amyloid β-peptides, tau (17), and α-synuclein (18, 19) *in vitro*. These molecules are biologically significant as mediators for signal-

* This work was supported by research grants from RIKEN Brain Science Institute and a grant-in-aid from the Ministry of Education, Culture, Sports, and Technology of Japan. The costs of publication of this article were defrayed in part by the payment of page charges. This article must therefore be hereby marked "*advertisement*" in accordance with 18 U.S.C. Section 1734 solely to indicate this fact.

‖ To whom correspondence should be addressed: Dept. of Neurology, Kyoto University Graduate School of Medicine, 54 Kawahara-cho, Shogoin, Sakyo-ku, Kyoto 606-8507, Japan. Tel.: 81-75-751-3770; Fax: 81-75-761-9780; E-mail: ryosuket@kuhp.kyoto-u.ac.jp.

[1] The abbreviations used are: ALS, amyotrophic lateral sclerosis; FALS, familial amyotrophic lateral sclerosis; SOD1, superoxide dismutase 1; FA, fatty acid; AA, arachidonic acid; MTS, 3-(4,5-dimethylthiazol-2-yl)-5-(3-carboxymethoxyphenyl)-2-(4-sulfophenyl)-2*H*-tetrazolium.

ing and inflammation during disease progression of neurodegeneration.

Here we investigated *in vitro* SOD1 aggregation affected by FAs to create an aggregation model system for FALS. We demonstrated that unsaturated FAs promote self-assembly and cytotoxic aggregate formation of SOD1. Aggregation by FAs is strongly correlated with structural instability and FA binding activity of SOD1, which may have significant implications in FALS.

EXPERIMENTAL PROCEDURES

Expression, Purification, and Characterization of Recombinant SOD1 Proteins—pcDNA3-SOD1 (20) was digested with EcoRV and XhoI and subcloned into blunted NcoI and XhoI sites of pET-15(b) (Novagen) to construct the expression plasmid. Expression of recombinant SOD1 proteins was induced in BL21(DE3)pLysS by adding 1 mM isopropyl 1-thio-β-D-galactopyranoside, 0.1 mM $CuCl_2$, and 0.1 mM $ZnCl_2$ until cells were grown to 0.6 absorbance unit at 600 nm, and then bacterial cells were further cultured at 23 °C for 6 h. Cells were pelleted and resuspended in TNE buffer (50 mM Tris-HCl, pH 8.0, 150 mM NaCl, and 0.1 mM EDTA) supplemented with protease inhibitor mixture (Roche Applied Science). Cells were then disrupted by sonication. Insoluble materials were removed by centrifugation at 10,000 × *g* for 30 min. Supernatant was collected for further purification. Purification was performed according to Hayward *et al.* (11), with minor modifications. Briefly, ammonium sulfate powder was added to the supernatant to 65% saturation with gentle stirring on ice. The supernatant, after centrifugation at 10,000 × *g* for 30 min, was directly loaded for phenyl-Sepharose (Amersham Biosciences) column chromatography. The column was thoroughly washed with TNE buffer containing 2 M ammonium sulfate. Proteins were eluted using a linearly decreasing salt gradient. SOD1 activity measurement using a xanthine/xanthine oxidase-based method (21) identified fractions containing SOD1. Activity fractions were desalted by ultrafiltration using a centricon filter (Millipore). SOD1 was re-metallated as described previously (22). The proteins were then loaded onto a Q-Sepharose (Amersham Biosciences) anion exchange column and eluted using a linearly increasing salt gradient toward a buffer containing 200 mM NaCl and 10 mM Tris-HCl, pH 8.0. Fractions containing SOD1 were pooled and concentrated. Homogeneity of SOD1 was >95%, as verified by SDS-PAGE with Coomassie Brilliant Blue staining. Specific activity of the purified enzymes was assayed and calculated by bovine SOD1 (Cayman) or human SOD1 purified from erythrocytes (Sigma-Aldrich) as standards. Fully metallated SOD1 was delipidated using hydroxyalkoxypropyl dextran type III (Sigma-Aldrich) as described previously (19) before de-metallation. Metal-deficient apo-enzymes were prepared as described previously (23), and loss of enzyme activity was confirmed after de-metallation. The metal content of purified enzymes was estimated as described previously (22).

Oligomerization of SOD1—A stock solution of 25 mM FAs was prepared in 0.01 M NaOH containing 25 μM butylated hydroxytoluene. SOD1 proteins were filtered through Microcon YM-100 (100-kDa cutoff) filters (Millipore) to remove high molecular mass SOD1 before oligomerization. FAs were added directly to preincubated SOD1 at 37 °C in 50 mM phosphate buffer, pH 7.2, containing 150 mM NaCl and 0.1 mM EDTA and further incubated at the same temperature.

SDS-PAGE and Western Blotting—For detection of SOD1 oligomers, SDS-PAGE was performed under non-reducing conditions using 12.5% polyacrylamide gels. After oligomerization of SOD1, protein samples were prepared in SDS-PAGE loading buffer (62.5 mM Tris-HCl, pH 6.8, 1% SDS, 5% glycerol, and 0.007% bromphenol blue) in the absence of β-mercaptoethanol and then boiled at 95 °C for 3 min before loading. Western blotting was performed as described previously (24). Briefly, proteins were transferred to Hybond ECL nitrocellulose membranes (Amersham Biosciences), followed by UV cross-linking, boiling membranes in 2% SDS and 50 mM Tris, pH 7.6, for 10 min, and extensive washing in Tris-buffered saline. For detection of SOD1, rabbit anti-SOD1 antibody (Stressgen) was used.

Glycerol Density Gradient Centrifugation and Densitometric Analysis—A glycerol linear gradient of 10–40% was prepared in a centrifuge tube. Formation of the SOD1 oligomer was performed as described above. Approximately 200 μl of incubated SOD1 was layered onto a glycerol cushion and separated by centrifugation with a SW41Ti rotor (Beckman) at 35,000 rpm for 15 h. In a parallel experiment, protein standards (Amersham Biosciences) were separated simultaneously in order to calibrate fractions. Fractions were subjected to SDS-PAGE under non-reducing conditions, and then Western blotting was performed. Western blot images were analyzed using image analysis software (Scion Image Beta 4.02; Scion Corp.).

Solid-phase Oleic Acid Binding—Sodium salt of oleic acid (Sigma-Aldrich) was coupled to EAH-Sepharose (Amersham Biosciences) by 1-ethyl-3-(3-dimethylaminopropyl)-carbodiimide (Pierce) to prepare oleate-Sepharose according to Peters *et al.* (25). Oleic acid coupling was verified by binding bovine serum albumin and recombinant α-synuclein protein. Mock-Sepharose was prepared from EAH-Sepharose by blocking coupling ligand with 1 M acetic acid. For the binding assay, 200 ng of Microcon-filtered protein was incubated with oleate-Sepharose or mock-Sepharose in 400 μl of phosphate-buffered saline containing 0.1 mM EDTA at 37 °C for 30 min with agitation. Protein bound to Sepharose was settled on a spun column and washed extensively with phosphate-buffered saline. The bound protein was then eluted with 50% ethanol. Eluates were subjected to SDS-PAGE and Western blotting.

Transmission Electron Microscopy—SOD1 proteins (40 μM) were incubated at 37 °C for 24 h in 50 mM phosphate buffer (pH 7.2) containing 150 mM NaCl and 0.1 mM EDTA supplemented with 100 μM arachidonic acid. The samples were absorbed to a glow-charged supporting membrane on 400-mesh grids and fixed by floating on 2.5% glutaraldehyde and 4% paraformaldehyde in 0.1 M phosphate buffer for 5 min. After three washes with distilled water, samples were negatively stained by 2% sodium phosphotungstic acid and dried. Specimens were observed in a LEO 912AB electron microscope (LEO Electron Microscopy), operated at 100 kV.

Toxicity Assay—Cytotoxicity of protein aggregates was measured as described previously (26, 27). In brief, neuro2a mouse neuroblastoma cells were maintained in Dulbecco's modified Eagle's medium with 10% fetal bovine serum and 2 mM glutamine in 5% CO_2 at 37 °C. Cells were differentiated in serum-free Dulbecco's modified Eagle's medium with 0.3 mM dibutylyl cAMP before use. Cells were plated at 30,000 cells/well in 96-well plates and differentiated overnight. The medium was removed, and prepared SOD1 aggregates were added in new medium without phenol red. After incubation for 18 h at 37 °C, the cells were assayed using an MTS reduction assay kit (Promega). Another plate also treated as described above was stained for 1 min with trypan blue, and stained cells were counted as dead cells.

RESULTS

Unsaturated Fatty Acids Promote Self-assembly of SOD1s—We expressed and homogeneously purified recombinant human SOD1s from the bacterial expression system (Fig. 1*A*). The purified wild-type and G93A enzymes showed comparable specific activity; however, A4V mutant showed ~56% activity compared with that of wild-type enzyme (Fig. 1*B*). The zinc ion content of the purified enzymes showed almost full occupancy; however, copper ion content of A4V was 54.5% of the wild-type level (Fig. 1*C*). Specific activity was correlated with copper ion occupancy of purified enzyme, indicating proper metal loading in the active site.

We next examined the effect of long-chain FAs on oligomerization of SOD1 proteins. Wild-type and mutant (A4V and G93A) SOD1 were incubated with various concentrations of arachidonic acid (AA) as described under "Experimental Procedures." After incubation, oligomerized SOD1 was subjected to SDS-PAGE and then detected by Western blotting. Under reducing conditions, mainly bands of ~16 and 38 kDa, corresponding to monomer and dimmer sizes of SOD1, respectively, were detected (Fig. 2*A*). In contrast, under non-reducing conditions, smeared patterns of >50 kDa in size were supposed to be SOD1 oligomers (Fig. 2*A*). These observations suggest that disulfide bonds maintained SOD1 oligomers. Thus, non-reducing SDS-PAGE was thought to be an efficient method to detect SOD1 oligomers and aggregates. Among the holo-enzymes, wild-type and G93A were not oligomerized; instead, they segregated as monomer and dimer size bands (Fig. 2*B*, *top panel*). After incubation with >100 μM AA, holo-A4V showed a faint smear pattern that was seen from 50 kDa to near the stacking gel range beside monomer- and dimer-size bands (Fig. 2*B*, *top panel*). In contrast, all metal-deficient enzymes, regardless of mutations, were oligomerized in the presence of >30 μM AA

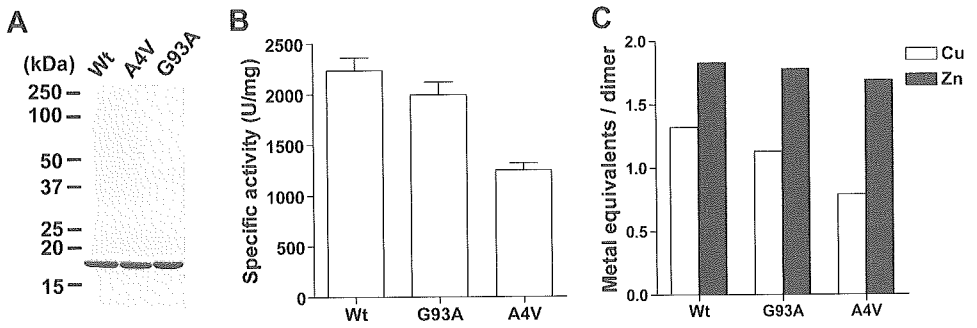

FIG. 1. **Characterization of purified recombinant SOD1s.** *A*, purified SOD1s were separated using SDS-PAGE and stained with Coomassie Brilliant Blue. *B*, dismutase activity of the purified SOD1s was assayed by the xanthine/xanthine oxidase-based method. One unit of the activity is defined as the amount of enzyme needed to exhibit 50% of dismutation of the superoxide radicals. *C*, metal content of the purified SOD1s was measured using 4-pyridylazoresorcinol assay in 6 M guanidine-HCl.

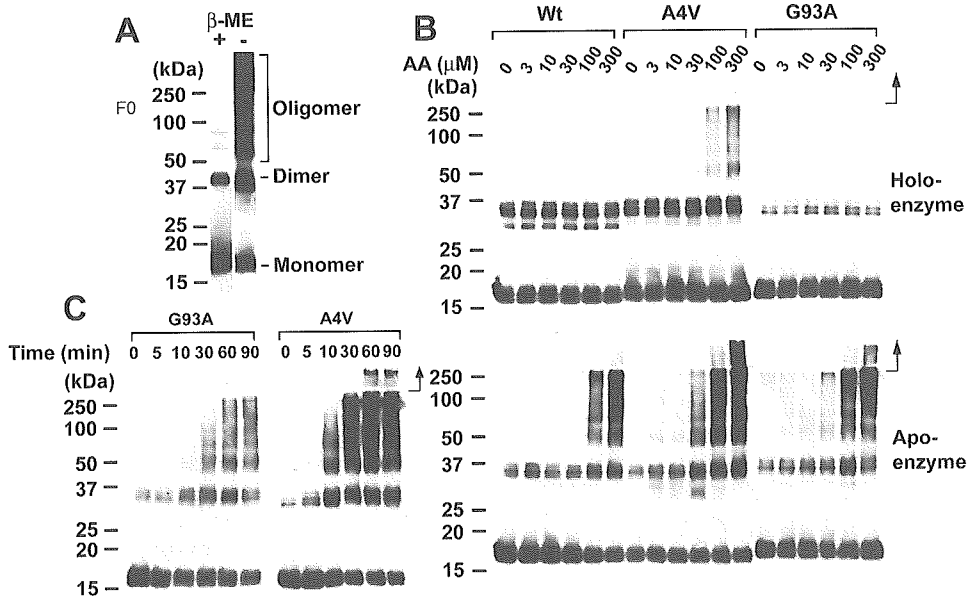

FIG. 2. **Arachidonic acid promotes SOD1 oligomerization.** *A*, FA-inducing oligomers of SOD1 were separated using SDS-PAGE with or without β-mercaptoethanol. *B*, apo-enzymes of SOD1 mutants (2.5 μM) were incubated at 37 °C in the presence of 100 μM AA. At each time point, aliquots were placed on ice to stop the reaction. *C*, purified holo- or apo-SOD1 proteins (2.5 μM) were incubated at 37 °C for 90 min in the presence of the indicated AA concentration. Incubated proteins were mixed directly with SDS-PAGE treatment buffer without reducing agents and boiled. SDS-PAGE was performed under non-reducing conditions. Proteins were detected by Western blotting as described under "Experimental Procedures." *Arrows* indicate the position of stacking gels.

(Fig. 2*B*, *bottom panel*). Apo-enzymes demonstrated higher oligomerization propensity than holo-enzymes depending on AA concentration (Fig. 2*B*). Thus, AA efficiently promoted oligomerization of SOD1s.

Next, we performed a time-course analysis of SOD1 oligomerization in the presence of AA. Metal-deficient G93A and A4V were oligomerized in a time-dependent manner (Fig. 2*C*). Maximum oligomerization was reached within 60 min of incubation in the presence of AA (Fig. 2*C*).

We then examined the effect that various FAs, including stearic acid, oleic acid, linoleic acid, and AA, have on SOD1 oligomerization. Unsaturated FAs, including oleic acid, linoleic acid, and AA, promoted SOD1 oligomerization (Fig. 3). However, saturated FAs and stearic acid had little effect on SOD1 oligomerization (Fig. 3). SOD1 oligomerization induced by FAs required at least monounsaturated FAs. This result may reflect the difference of solubility between unsaturated and saturated FAs in the buffer.

We verified the formation of SOD1 oligomers using a 10–40% glycerol density gradient centrifugation because presumable artifacts after detection of SOD1 oligomers using non-reducing SDS-PAGE may have remained. After fractionation, we could not observe high molecular mass SOD1 oligomers

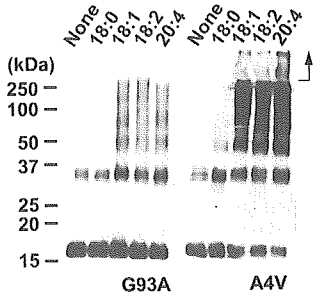

FIG. 3. **Unsaturated fatty acids affect oligomerization of SOD1.** Apo-enzymes of SOD1 mutants were incubated at 37 °C for 90 min in the presence of FAs at concentrations of 100 μM: 18:0, stearic acid; 18:1, oleic acid; 18:2, linoleic acid; and 20:4, arachidonic acid. *Arrows* indicate the position of stacking gels.

from the incubated sample in the absence of AA; fractions were <67 kDa and potentially represented monomer and dimer states (Fig. 4*A*, *top panel*). In contrast, we detected high molecular mass oligomers in fractions of >440 kDa from the incubated sample in the presence of AA (Fig. 4*A*, *bottom panel*). Under these conditions, SOD1 with molecular mass of <67 kDa was dramatically decreased compared with the sample incu-

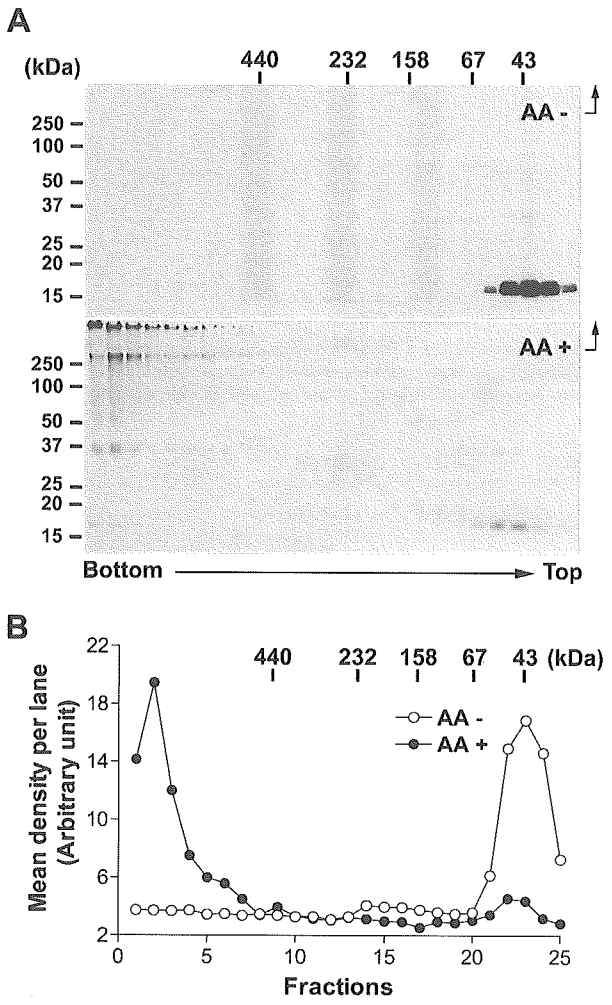

FIG. 4. **Glycerol density gradient centrifugation and densitometric analysis of SOD1 oligomers.** *A*, apo-A4V (2.5 μM) was incubated at 37 °C for 90 min in the absence or presence of 100 μM AA before loading on the glycerol cushion. After centrifugation, fractions were collected from the bottom of the tubes and then subjected to SDS-PAGE under non-reducing conditions. SOD1 proteins were detected by Western blotting. *B*, for densitometric analysis, we measured mean density per lane after background subtraction. Total mean density was similar under each condition, by calculating the mean density of visible lanes (*lanes 1–8* for oligomers and *lanes 21–25* for dimer or monomer). *Arrows* indicate the position of stacking gels.

bated in the absence of AA (Fig. 4*A*, *bottom panel*). Although oligomers of >440 kDa were fractionated by the glycerol density gradient centrifugation, these were detected as monomer, dimer, and smeared high molecular mass bands that reached stacking gels under non-reducing SDS-PAGE (Fig. 4*A*, *bottom panel*). This indicates oligomers are partly disrupted during the boiling of the SDS-PAGE loading buffer. We next performed densitometric analysis from Western blotting images to estimate the amount of oligomerized SOD1 (Fig. 4*B*). The resulting image analysis found that immunoreactivity for oligomers was ~80% of the total immunoreactivity.

Structural Instability of SOD1 Is Correlated to Oligomerization Propensity and FA Binding—We showed the FA-induced oligomerization propensity of apo-SOD1s was higher than that of holo-SOD1. This implies that protein stability might be strongly associated with FA-induced oligomerization propensity. Among the holo-enzymes, wild-type and G93A were not oligomerized under our experimental conditions (Fig. 2*B*, *top panel*). To examine the correlation between oligomerization propensity and protein stability of holo-enzymes, holo-SOD1 was heated and then oligomerized by AA. In the absence of AA,

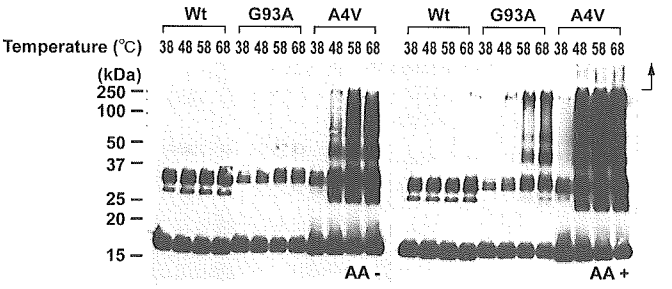

FIG. 5. **Thermally destabilized SOD1 mutants show a high oligomerization propensity.** Holo-enzymes were heat-treated at the indicated temperatures for 30 min before addition of 100 μM AA and then further incubated at 37 °C for 1 h. SDS-PAGE was performed under non-reducing conditions. Proteins were detected by Western blotting as described under "Experimental Procedures." *Arrows* indicate the position of stacking gels.

only heat-treated A4V was oligomerized (Fig. 5, *left panel*). In the presence of AA, heat-treated G93A and A4V were highly aggregated, but under the same conditions, wild-type SOD1 was not (Fig. 5, *right panel*). Oligomerization was observed above 58 °C for G93A and above 48 °C for A4V (Fig. 5, *right panel*). In the previous study, A4V was more unstable than G93A for heat treatment analyzed by differential scanning calorimetry (12). This result suggests that structural instability is strongly correlated with oligomerization propensity induced by FAs.

Although we showed that FAs promoted SOD1 oligomerization, the mechanism is not perfectly understood. Similarly, unsaturated FAs oligomerize α-synuclein and tau. In the case of α-synuclein and tau, FAs were bound to proteins, which suggested that oligomerization mechanisms underlie the FA binding characteristics of protein. To examine whether SOD1 binds to FAs, we carried out a solid-phase oleic acid binding assay. Among the holo-enzymes, very small amounts of holo-A4V were bound to the oleate-Sepharose column, whereas wild-type and G93A were not (Fig. 6*A*). All of the apo-enzymes were bound to oleate-Sepharose, regardless of their mutations (Fig. 6*A*). In contrast, bound proteins were not observed in mock-Sepharose (Fig. 6*A*). Nearly all of the input amounts of metal-deficient proteins were bound, which was estimated by 50% input. This finding suggests that metal-deficient SOD1 proteins strongly bind to FAs. We next examined whether heat-treated holo-enzymes bind to FAs. Apo-enzymes were used as control binding. Heat-treated SOD1 mutant (G93A) at 58 °C and 68 °C was bound to FAs, whereas wild-type was not (Fig. 6*B*). The results of the FA binding assay were strongly correlated with the oligomerization propensity of SOD1. These findings suggest that FA binding alters the conformation of SOD1 to form oligomers.

FA-induced SOD1 Aggregates Result in Granular Morphology and Are Cytotoxic—We analyzed the ultrastructure of SOD1 aggregates by electron microscope. SOD1 proteins (~40 μM) were incubated in the presence of 100 μM AA at 37 °C for 24 h. Holo-enzymes were heated at 50 °C for 30 min before incubation in the presence of AA. After incubation, granular aggregates were observed in all of apo-enzymes and heat-treated SOD1 mutants (Fig. 7*A*). In contrast, no visible materials were found in wild-type holo-SOD1s, even though they were heat-treated (Fig. 7*A*). The morphology of the aggregates was round or amorphous large granules composed of clustered small granules (Fig. 7*A*). We could not observe any visible protein aggregates in the samples incubated without AA, except in apo-A4V, which revealed a fibril structure (data not shown).

We next examined the effect of FA-induced aggregates on cell

viability of differentiated neuro2a cells. Aggregates of SOD1s were formed using the same methods as described for observation under an electron microscope. Aliquots incubated in the presence or absence of AA were diluted in the culture medium, which was directly added to differentiated neuro2a cells. After incubation for 18 h, toxicity was assessed with MTS reduction (Fig. 7*B*) and trypan blue staining (Fig. 7*C*). The presence of the granular aggregates formed by AA from Apo-SOD1s and heat-treated SOD1 mutants significantly reduced cell viability (Fig. 7, *B* and *C*). In contrast, no significant decrease of viability was detected when the cells were exposed either to incubated proteins in the absence of AA or to the buffer solutions used to form the aggregates in the absence of added protein (Fig. 7, *B* and *C*). These findings suggest that FA-induced SOD1 aggregates were highly toxic to the cells.

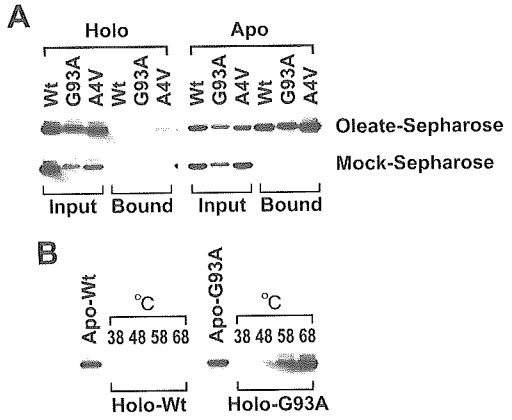

FIG. 6. **Solid-phase oleic acid binding assay shows apo-SOD1 or thermally destabilized SOD1 bound to oleate-Sepharose.** *A*, solid-phase binding assay was performed as described under "Experimental Procedures." Approximately 50% input (100 ng of proteins) was electrophoresed to estimate the quantity of FA binding SOD1. *B*, holo-SOD1s (wild-type and G93A) were thermally destabilized at the indicated temperatures for 30 min and then directly loaded on oleate-Sepharose. Apo-enzymes were used as positive controls for oleic acid binding.

DISCUSSION

Numerous neurodegenerative diseases are accompanied by highly insoluble inclusions of protein aggregates within characteristic neuronal populations. In the case of FALS, the protypical Lewy body-like hyaline inclusions, composed largely of granule-coated fibrils of SOD1-insoluble filaments, have been detected in the spinal cord of FALS patients with SOD1 gene mutations (5, 28). Although there has been controversy about whether such inclusions are a cause or a consequence of the neuronal degeneration, accumulating evidence suggests that aggregates formed via misfolded proteins, especially soluble oligomeric assemblies, may cause cell injury (29–31). Moreover, cytotoxicity of protein aggregates may have common features because granular aggregates form non-pathological proteins that can also be toxic (26). These findings suggest the avoidance of protein aggregation may be crucial for therapy of

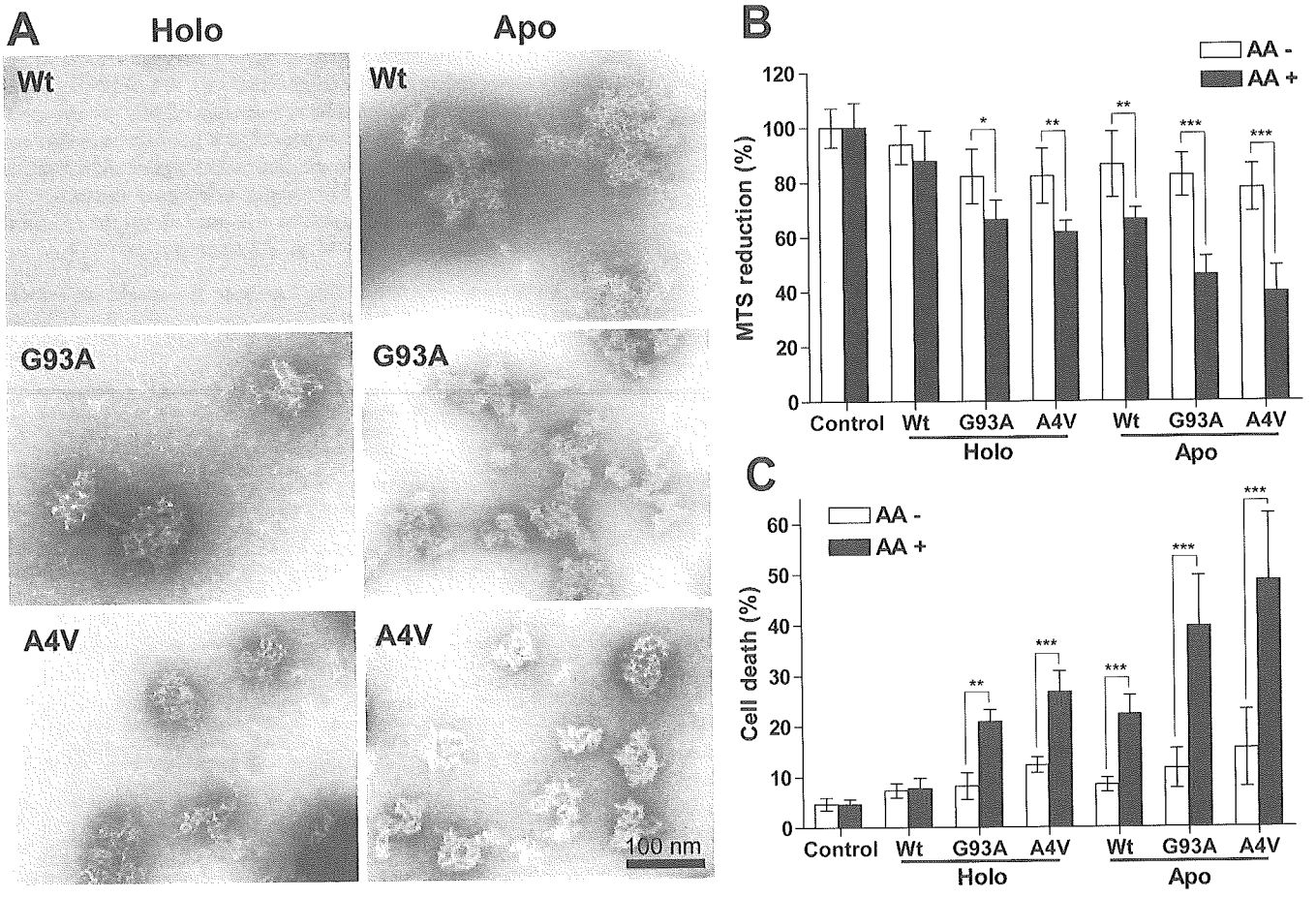

FIG. 7. **SOD1 aggregates and their cytotoxicity for the differentiated neuro2a cells.** Holo-SOD1s were pre-heated at 50 °C for 30 min before incubation with AA. SOD1 proteins (40 μM) were incubated in the presence of 100 μM AA at 37 °C for 24 h before observation under an electron microscope (*A*). Differentiated neuro2a cells were directly exposed for 18 h in medium containing incubated aliquots of SOD1s with or without arachidonic acid. The concentration of SOD1 in the culture medium was 4 μM. Buffer and AA carryover in the culture medium was controlled. Cytotoxicity was assessed using an MTS reduction assay (*B*) and trypan blue exclusion staining (*C*). The results were analyzed by two-way analysis of variance. The values are the means ± S.D. ($n = 6$). *, $p < 0.05$; **, $p < 0.01$; ***, $p < 0.001$.

conformational diseases including FALS.

In the present study, we demonstrated that unsaturated FAs promoted SOD1 oligomerization at physiological pH. SOD1 oligomers were detected by SDS-PAGE under non-reducing conditions. Although immunoreactivity for SOD1 oligomers was decreased in SDS-PAGE under reducing conditions, SOD1 oligomers were considerably SDS-resistant under non-reducing conditions. Based on this method, we found that apo-SOD1 proteins were highly oligomerized by AA compared with holo-SOD1 proteins in time-dependent and FA concentration-dependent manners (Fig. 2, *B* and *C*). Metal-deficient SOD1s may be representative of misfolding intermediates for their oligomeric assemblies because they are oligomerized independent of their mutations. These findings suggest that metal-deficient SOD1 proteins have a high oligomerization propensity, which is consistent with previous studies (9, 10, 13, 32). Moreover, heating of holo-SOD1 mutants increased the tendency to form oligomer complexes, especially in the presence of AA; however, the wild-type holo-SOD1 did not form oligomers, even after heating to 68 °C and exposure to AA (Fig. 5). This finding suggests that mutations of SOD1 primarily affect their conformation. Our time-course analysis of oligomerization demonstrates that FAs induced the oligomerization process fairly rapidly. We could detect oligomers within 1 h of incubation in the presence of AA (Fig. 1*C*). Glycerol density gradient centrifugation analysis showed that oligomer species were roughly estimated to be >80% of the total SOD1 after a 90-min incubation in the presence of AA (Fig. 4). The conversion efficiency and the speed of oligomer formation may be considered as supportive evidence that these reactions occur *in vivo*.

Aggregations of misfolded proteins are primarily affected by their mutations, especially in inherited conformational diseases. Mutant proteins in conformational diseases have a common characteristic of easily unfolding in a physiological condition and favoring aggregate formation. Protein aggregation has also been shown to be modulated by several factors, including protein concentration, pH, and interactions with other elements such as lipid molecules. It has been reported that FAs stimulated the polymerization of amyloid β-peptides, tau (17, 33), and α-synuclein (18, 19) *in vitro*. These studies suggest that FAs play a pivotal role as nucleates in the self-assembly of misfolded proteins. Although the precise mechanism of how lipid molecules accelerate protein aggregation has not been elucidated, it has been proposed that lipid-bound proteins change their conformation or anionic surfaces, presenting as micelles or vesicles, which can serve to nucleate aggregate formation (18, 34, 35). We confirmed that apo-SOD1s or heat-treated holo-SOD1 mutants were bound to oleic acid (Fig. 6). The FA binding properties of SOD1s were strongly correlated to their conformational instability. These results are consistent with the notion that misfolding intermediates of SOD1 caused by mutations or metal loss may be facilitated by FAs to form oligomeric structures. Another possible mechanism is protein oxidation by FAs. Oxidation also enhances misfolding and aggregation of SOD1 (32). In particular, FAs can lead to the production of radicals because they are easily peroxidized by auto-oxidation to generate peroxyl radicals. However, we could not inhibit SOD1 oligomerization using even a considerable amount of radical scavenger (data not shown). Moreover, oxidized derivatives of FAs also induced SOD1 oligomerization to a similar extent with fresh FAs (data not shown). This finding suggests that oxidation or oxidative damage of SOD1 does not directly drive SOD1 oligomerization. Rather, it is most likely to be associated with a SOD1-destabilizing event.

Recently, several studies for *in vitro* aggregation of SOD1 have been published. Aggregation of SOD1 can be induced by metal-catalyzed oxidation (32), trifluoroethanol, or heat treatment (10), which induces oxidative modification or protein destabilization. This indicates that structurally unstable SOD1 has an influence on its aggregate formation *in vitro*. Crystallographic studies suggest that metal-deficient SOD1 forms an amyloid-like assembly caused by non-native conformational changes and permits dimer interaction (36, 37). This amyloid-like structure was represented by prolonged incubation of SOD1 at acidic pH (9). In the present study, ultrastructural analysis showed that the FA-inducing aggregates had round or amorphous morphology with clustered tiny spherical aggregates (Fig. 7*A*). They resemble pre-fibrillar aggregates of the N-terminal domain of *Escherichia coli* HypF protein or aggregates of the Src homology 3 domain of cytosolic phosphatidylinositol 3-kinase as reported by Stefani and co-workers (26). They demonstrated that granular aggregates of proteins, even non-pathological proteins, are cytotoxic when applied externally (26). Our data also demonstrate that granular aggregates of SOD1s reveal significant cytotoxicity (Fig. 7, *B* and *C*). Although the cytotoxic mechanism of the aggregates is not completely understood, it has been proposed that such pre-fibrillar intermediates may lead to cytotoxicity by permeabilization of the membrane bilayer (38, 39).

The present findings may provide considerable pathological implication for FALS. Lipid molecules such as FAs may be positive modulators for misfolded protein aggregations. Most misfolded proteins including SOD1 mutants are rapidly degraded by the ubiquitin-proteasome system. Unsaturated FAs may promote misfolded protein aggregations before they are degraded. In addition, cytotoxic aggregate formation of SOD1 may require FAs because granular aggregates structures were markedly observed in SOD1s incubated with AA. Although it is not clear whether the cytotoxic aggregates of SOD1s are generated intracellularly, we have provided a protein aggregation model system to help understand the pathological significance of FAs as a positive modulator for the aggregate formation in FALS. We believe that our system will contribute to efficient drug screening for inhibitors of SOD1 aggregation.

Acknowledgment—We thank Dr. Toshihide Kobayashi for critical advice and helpful discussions.

REFERENCES

1. Deng, H. X., Hentati, A., Tainer, J. A., Iqbal, Z., Cayabyab, A., Hung, W. Y., Getzoff, E. D., Hu, P., Herzfeldt, B., Roos, R. P., Warner, C., Deng, G., Soriano, E., Smyth, C., Parge, H. E., Ahmed, A., Roses, A. D., Hallewell, R., Pericak-Vance, M. A., and Siddique, T. (1993) *Science* **261,** 1047–1051
2. Rosen, D. R., Siddique, T., Patterson, D., Figlewicz, D. A., Sapp, P., Hentati, A., Donaldson, D., Goto, J., O'Regan, J. P., Deng, H. X., Rahmani, Z., Krizus, A., McKenna-Yasek, D., Cayabyab, A., Gaston, S., Tanzi, R., Halperin, J. J., Herzfeldt, B., Van den Berg, R., Hung, W., Bird, T., Deng, G., Mulder, D. W., Smith, C., Laing, N. G., Soriano, E., Pericak-Vance, M. A., Haines, J., Rouleau, G. A., Gusella, J., Horvitz, H. R., and Brown, R. H., Jr. (1993) *Nature* **362,** 59–62
3. Shibata, N., Asayama, K., Hirano, A., and Kobayashi, M. (1996) *Dev. Neurosci.* **18,** 492–498
4. Bruijn, L. I., Becher, M. W., Lee, M. K., Anderson, K. L., Jenkins, N. A., Copeland, N. G., Sisodia, S. S., Rothstein, J. D., Borchelt, D. R., Price, D. L., and Cleveland, D. W. (1997) *Neuron* **18,** 327–338
5. Kato, S., Hayashi, H., Nakashima, K., Nanba, E., Kato, M., Hirano, A., Nakano, I., Asayama, K., and Ohama, E. (1997) *Am. J. Pathol.* **151,** 611–620
6. Shibata, N., Hirano, A., Kobayashi, M., Dal Canto, M. C., Gurney, M. E., Komori, T., Umahara, T., and Asayama, K. (1998) *Acta Neuropathol.* **95,** 136–142
7. Watanabe, M., Dykes-Hoberg, M., Culotta, V. C., Price, D. L., Wong, P. C., and Rothstein, J. D. (2001) *Neurobiol. Dis.* **8,** 933–941
8. Wang, J., Xu, G., Gonzales, V., Coonfield, M., Fromholt, D., Copeland, N. G., Jenkins, N. A., and Borchelt, D. R. (2002) *Neurobiol. Dis.* **10,** 128–138
9. DiDonato, M., Craig, L., Huff, M. E., Thayer, M. M., Cardoso, R. M., Kassmann, C. J., Lo, T. P., Bruns, C. K., Powers, E. T., Kelly, J. W., Getzoff, E. D., and Tainer, J. A. (2003) *J. Mol. Biol.* **332,** 601–615
10. Stathopulos, P. B., Rumfeldt, J. A., Scholz, G. A., Irani, R. A., Frey, H. E., Hallewell, R. A., Lepock, J. R., and Meiering, E. M. (2003) *Proc. Natl. Acad. Sci. U. S. A.* **100,** 7021–7026
11. Hayward, L. J., Rodriguez, J. A., Kim, J. W., Tiwari, A., Goto, J. J., Cabelli, D. E., Valentine, J. S., and Brown, R. H., Jr. (2002) *J. Biol. Chem.* **277,** 15923–15931

12. Rodriguez, J. A., Valentine, J. S., Eggers, D. K., Roe, J. A., Tiwari, A., Brown, R. H., Jr., and Hayward, L. J. (2002) *J. Biol. Chem.* **277,** 15932–15937
13. Lindberg, M. J., Tibell, L., and Oliveberg, M. (2002) *Proc. Natl. Acad. Sci. U. S. A.* **99,** 16607–16612
14. Johnston, J. A., Dalton, M. J., Gurney, M. E., and Kopito, R. R. (2000) *Proc. Natl. Acad. Sci. U. S. A.* **97,** 12571–12576
15. Urushitani, M., Kurisu, J., Tateno, M., Hatakeyama, S., Nakayama, K., Kato, S., and Takahashi, R. (2004) *J. Neurochem.* **90,** 231–244
16. Shinder, G. A., Lacourse, M. C., Minotti, S., and Durham, H. D. (2001) *J. Biol. Chem.* **276,** 12791–12796
17. Wilson, D. M., and Binder, L. I. (1997) *Am. J. Pathol.* **150,** 2181–2195
18. Sharon, R., Goldberg, M. S., Bar-Josef, I., Betensky, R. A., Shen, J., and Selkoe, D. J. (2001) *Proc. Natl. Acad. Sci. U. S. A.* **98,** 9110–9115
19. Sharon, R., Bar-Joseph, I., Frosch, M. P., Walsh, D. M., Hamilton, J. A., and Selkoe, D. J. (2003) *Neuron* **37,** 583–595
20. Urushitani, M., Kurisu, J., Tsukita, K., and Takahashi, R. (2002) *J. Neurochem.* **83,** 1030–1042
21. Fried, R. (1975) *Biochimie (Paris)* **57,** 657–660
22. Crow, J. P., Sampson, J. B., Zhuang, Y., Thompson, J. A., and Beckman, J. S. (1997) *J. Neurochem.* **69,** 1936–1944
23. Boissinot, M., Karnas, S., Lepock, J. R., Cabelli, D. E., Tainer, J. A., Getzoff, E. D., and Hallewell, R. A. (1997) *EMBO J.* **16,** 2171–2178
24. Bartnikas, T. B., and Gitlin, J. D. (2003) *J. Biol. Chem.* **278,** 33602–33608
25. Peters, T., Jr., Taniuchi, H., and Anfinsen, C. B., Jr. (1973) *J. Biol. Chem.* **248,** 2447–2451
26. Bucciantini, M., Giannoni, E., Chiti, F., Baroni, F., Formigli, L., Zurdo, J., Taddei, N., Ramponi, G., Dobson, C. M., and Stefani, M. (2002) *Nature* **416,** 507–511
27. Kayed, R., Head, E., Thompson, J. L., McIntire, T. M., Milton, S. C., Cotman, C. W., and Glabe, C. G. (2003) *Science* **300,** 486–489
28. Kato, S., Saito, M., Hirano, A., and Ohama, E. (1999) *Histol. Histopathol.* **14,** 973–989
29. Walsh, D. M., Hartley, D. M., Kusumoto, Y., Fezoui, Y., Condron, M. M., Lomakin, A., Benedek, G. B., Selkoe, D. J., and Teplow, D. B. (1999) *J. Biol. Chem.* **274,** 25945–25952
30. Hartley, D. M., Walsh, D. M., Ye, C. P., Diehl, T., Vasquez, S., Vassilev, P. M., Teplow, D. B., and Selkoe, D. J. (1999) *J. Neurosci.* **19,** 8876–8884
31. Tateno, M., Sadakata, H., Tanaka, M., Itohara, S., Shin, R. M., Miura, M., Masuda, M., Aosaki, T., Urushitani, M., Misawa, H., and Takahashi, R. (2004) *Hum. Mol. Genet.* **13,** 2183–2196
32. Rakhit, R., Cunningham, P., Furtos-Matei, A., Dahan, S., Qi, X. F., Crow, J. P., Cashman, N. R., Kondejewski, L. H., and Chakrabartty, A. (2002) *J. Biol. Chem.* **277,** 47551–47556
33. Gamblin, T. C., King, M. E., Kuret, J., Berry, R. W., and Binder, L. I. (2000) *Biochemistry* **39,** 14203–14210
34. Necula, M., Chirita, C. N., and Kuret, J. (2003) *J. Biol. Chem.* **278,** 46674–46680
35. Chirita, C. N., Necula, M., and Kuret, J. (2003) *J. Biol. Chem.* **278,** 25644–25650
36. Elam, J. S., Taylor, A. B., Strange, R., Antonyuk, S., Doucette, P. A., Rodriguez, J. A., Hasnain, S. S., Hayward, L. J., Valentine, J. S., Yeates, T. O., and Hart, P. J. (2003) *Nat. Struct. Biol.* **10,** 461–467
37. Strange, R. W., Antonyuk, S., Hough, M. A., Doucette, P. A., Rodriguez, J. A., Hart, P. J., Hayward, L. J., Valentine, J. S., and Hasnain, S. S. (2003) *J. Mol. Biol.* **328,** 877–891
38. Caughey, B., and Lansbury, P. T. (2003) *Annu. Rev. Neurosci.* **26,** 267–298
39. Kayed, R., Sokolov, Y., Edmonds, B., McIntire, T. M., Milton, S. C., Hall, J. E., and Glabe, C. G. (2004) *J. Biol. Chem.* **279,** 46363–46366

Inactivation of *Drosophila* DJ-1 leads to impairments of oxidative stress response and phosphatidylinositol 3-kinase Akt signaling

Yufeng Yang*†, Stephan Gehrke*†, Md. Emdadul Haque*, Yuzuru Imai*, Jon Kosek*, Lichuan Yang‡, M. Flint Beal‡, Isao Nishimura§, Kazumasa Wakamatsu¶, Shosuke Ito¶, Ryosuke Takahashi, and Bingwei Lu*,**

*Department of Pathology, Stanford University School of Medicine, and Geriatric Research, Education and Clinical Center Veterans Affairs Palo Alto Health Care System, Palo Alto, CA 94304; ‡Department of Neurology, Cornell University Medical College, 525 East 68th Street, New York, NY 10021; §Division of Regulation of Macromolecular Functions, Institute for Protein Research, Osaka University, 3-2 Yamadaoka, Suita, Osaka 565-0871, Japan; ¶Department of Chemistry, Fujita Health University School of Health Sciences, Toyoake, Aichi 470-1192, Japan; and Laboratory for Motor System Neurodegeneration, RIKEN Brain Science Institute, 2-1 Hirosawa, Wako-shi, Saitama 351-0198, Japan

Edited by Tak Wah Mak, University of Toronto, Toronto, Canada, and approved July 29, 2005 (received for review June 3, 2005)

Parkinson's disease (PD) is the most common movement disorder characterized by dopaminergic dysfunction and degeneration. The cause of most PD cases is unknown, although postmortem studies have implicated the involvement of oxidative stress. The identification of familial PD-associated genes offers the opportunity to study mechanisms of PD pathogenesis in model organisms. Here, we show that DJ-1A, a *Drosophila* homologue of the familial PD-associated gene DJ-1, plays an essential role in oxidative stress response and neuronal maintenance. Inhibition of DJ-1A function through RNA interference (RNAi) results in cellular accumulation of reactive oxygen species, organismal hypersensitivity to oxidative stress, and dysfunction and degeneration of dopaminergic and photoreceptor neurons. To identify other genes that may interact with DJ-1A in regulating cell survival, we performed genetic interaction studies and identified components of the phosphatidylinositol 3-kinase (PI3K) Akt-signaling pathway as specific modulators of DJ-1A RNAi-induced neurodegeneration. PI3K signaling suppresses DJ-1A RNAi phenotypes at least in part by reducing cellular reactive oxygen species levels. Consistent with the genetic interaction results, we also found reduced phosphorylation of Akt in DJ-1A RNAi animals, indicating an impairment of PI3K Akt signaling by DJ-1A down-regulation. Together with recent findings in mammalian systems, these results implicate impairments of PI3K Akt signaling and oxidative stress response in DJ-1-associated disease pathogenesis. We also observed impairment of PI3K Akt signaling in the fly *parkin* model of PD, hinting at a common molecular event in the pathogenesis of PD. Manipulation of PI3K Akt signaling may therefore offer therapeutic benefits for the treatment of PD.

Parkinson's disease PI3K PTEN Akt signaling reactive oxygen species

Parkinson's disease (PD) is the most common movement disorder and the second most common neurodegenerative disease. The movement abnormality in PD arises from deficiency of brain dopamine (DA) contents and the degeneration of dopaminergic neurons in the substantia nigra. The most common forms of PD are sporadic with no known cause. Nevertheless, postmortem studies have identified common features associated with sporadic PD, including defects in mitochondrial complex I function, oxidative damage, and abnormal protein aggregation (1).

The contribution of genetic factors in the pathogenesis of PD, although initially controversial, has been firmly established by recent human genetic studies. At least 10 distinct loci (PARK1 to -11) have been linked to rare familial forms of PD (2). It is anticipated that understanding the molecular lesions associated with these familial PD (FPD) genes will shed light on the pathogenesis of the sporadic forms of the disease. To date, five unequivocal FPD genes have been molecularly cloned. These include -*Synuclein* (-Syn), Parkin, DJ-1, PINK-1, and dardarin. Biochemical and biophysical studies of -Syn and Parkin have primarily linked dysfunction of these genes to aberrant protein folding and ubiquitin-proteasome dysfunction. Intriguingly, *in vivo* genetic and *in vitro* cell culture studies have revealed their connection to mitochondrial dysfunction and oxidative stress, reinforcing the involvement of these processes in PD pathogenesis in general (3).

DJ-1 encodes a conserved protein belonging to the ThiJ PfpI DJ-1 superfamily. The exact molecular function of DJ-1 is still unclear. Human DJ-1 was initially discovered as a candidate oncoprotein that could transform cells in cooperation with activated *ras* (4), and it was later found as a component of an RNA-binding protein complex and was associated with male infertility (4–6). Under oxidative stress conditions, DJ-1 was modified by oxidation, and the modified form associated with mitochondria in cultured cells (7–10). Knocking down DJ-1 expression with small interfering RNA (siRNA) resulted in susceptibility to oxidative stress, endoplasmic reticulum stress, and proteasome inhibition (11). Recent analyses of DJ-1 knockout mice have shed light on the physiological function of DJ-1 in mammals. DJ-1-deficient mice were found to have nigrostriatal dopaminergic dysfunction, motor deficits, and hypersensitivity to the neurotoxin 1-methyl-4-phenyl-1,2,3,6-tetrahydropyrindine (MPTP) and oxidative stress stimuli (12–14). In mammalian cells, DJ-1 was found to regulate the phosphorylation status of protein kinase B (PKB) Akt through the tumor suppressor PTEN (15). The relevance of this novel finding of DJ-1 function to PD pathogenesis remains to be explored.

As an alternative approach to understanding the role of DJ-1 dysfunction in PD pathogenesis, we have used *Drosophila* as a model system. We inhibited the function of a *Drosophila* DJ-1 homologue (DJ-1A) by transgenic RNA interference (RNAi). DJ-1A RNAi flies show cellular accumulation of reactive oxygen species (ROS), hypersensitivity to oxidative stress, and degeneration of dopaminergic and photoreceptor neurons. Genetic interaction studies with candidate genes and pathways previously implicated in survival signaling led to the identification of genes in the PI3K Akt-signaling pathway as specific modifiers of DJ-1A-associated cell death phenotype. Consistent with the genetic interaction results, PI3K signaling was found to regulate cellular ROS levels, and we found that DJ-1A down-regulation leads to impairment of PI3K Akt signaling. Significantly, we found that dysfunction of *parkin*, another PD-associated gene, also led to impaired

This paper was submitted directly (Track II) to the PNAS office.

Abbreviations: DA, dopamine; DMC, dorsomedial cluster; PD, Parkinson's disease; RNAi, RNA interference; ROS, reactive oxygen species; TH, tyrosine hydroxylase; PKB, protein kinase B; PI3K, phosphatidylinositol 3-kinase; *Da*, *daughterless*; 3-AT, 3-amino-triazole; DCFH-DA, 2,7-dichlorofluorescein diacetate; DN, dominant-negative.

†Y.Y. and S.G. contributed equally to this work.

**To whom correspondence should be addressed. E-mail: bingwei@stanford.edu.

www.pnas.org cgi doi 10.1073 pnas.0504610102

PI3K Akt signaling. Our results implicate oxidative stress and impairment of PI3K Akt signaling as a general feature of PD pathogenesis and suggest new avenues for therapeutic intervention.

Experimental Procedures

Drosophila Genetics. Fly culture and crosses were performed according to standard procedures and raised at indicated temperatures. All general fly stocks and *GAL4* lines were obtained from the Bloomington *Drosophila* Stock Center. The other fly stocks have been described: *UAS-Akt* (16); *UAS-PI3Kp110* and *UAS-PI3Kp110 DN* (17); *UAS-PTEN* (18); and *UAS-tau V337M* (19). To generate *UAS-dsDJ-1A* and *UAS-dsDJ-1B* transgenics, genomic DNA cDNA hybrid constructs were generated as described (20). To make *UAS-DJ-1A*, *UAS-DJ-1B*, and *UAS-hDJ-1* transgenics, corresponding full-length cDNA was cloned into the *pUAST* vector. Details of the cloning steps are available upon request. Approximately 9 g of *pUAST* transgenic construct was mixed with 3 g of helper plasmid in 20 l of injection buffer. Standard procedures were followed for embryo injection and recovery of transgenic lines.

Molecular Biology. For RT PCR analysis, 2nd to 3rd instar larvae from the cross between *UAS-dsDJ-1A* and *Da-GAL4* were used to prepare total RNA by using an RNeasy Kit (Qiagen, Valencia, CA). Details of the quantitative RT PCR procedure were essentially as described (21). Antibodies against DJ-1A and DJ-1B were elicited in rabbits with recombinant proteins purified from bacteria culture expressing *pGEX-6P-1-DJ-1A* or *pGEX-6P-1-DJ-1B* vectors, which contain corresponding full-length cDNA inserts. Western blot analysis using these antibodies was performed as described (21), with each primary antibody used at 1:5,000 dilution. For Western blot analysis of Akt, *Da-GAL4* and *Da-GAL4 DJ-1A RNAi* animals were raised at 18°C from the larvae stage to obtain viable *Da-GAL4 DJ-1A RNAi* adult animals, because these animals die at larvae stage when raised at 25°C. Newly eclosed adult flies were transferred to 29°C to induce stronger RNAi. *Da-GAL4 dParkin RNAi* flies were raised at 29°C constantly. Fly head extracts were prepared for Western blot analysis with anti-Akt and anti-*p*-Akt (S505) antibodies (Cell Signaling Technology, Beverly, MA).

Histology and Immunohistochemistry. Sections of paraplast-embedded adult fly heads were prepared and processed as described (21). The sections were incubated in primary antibody overnight at 4°C, and subsequently processed by using the Vectastain Universal Elite ABC Kit (Vector Laboratories). The primary antibody used was anti-tyrosine hydroxylase (TH) polyclonal antibody (Pel-Freez Biologicals, 1:100). For the analysis of adult retina, eye sectioning and staining with toluidine blue was performed as described (22). Between four and five fly heads for each genotype per time point were examined, and each experiment was repeated at least once. The neuronal culture system was established and processed for immunofluorescence staining as described (21). For ROS staining of neuronal culture and adult fly brain, 2,7-dichlorofluorescein diacetate (DCFH-DA) (Molecular Probes) was used following the manufacturer's instructions.

DA Measurement. HPLC analysis of catecholamine levels was performed as described (23, 24). For sample preparation, adult male fly heads were dissected out and homogenized in 0.1 M perchloric acid (generally 50 l per four or five heads) by using a motorized hand-held tissue grinder. The homogenate was frozen immediately on dry ice and stored at 80°C before HPLC analysis.

Oxidative Stress Assay. For oxidative stress assay, flies were kept in plastic vials with a piece of Kimwipe paper soaked with 1% H_2O_2 or 100 mM 3-amino-triazole (3-AT) in Schneider's Medium. The vials were kept at 25°C in a shielded box. Fresh H_2O_2 or 3-AT was added to the paper daily with a syringe. Mortality was recorded every 12 h or at shorter intervals.

Results

Specific Knockdown of _Drosophila DJ-1A_ Expression by Transgenic RNAi. In the sequenced *Drosophila* genome, there are two previously uncharacterized genes, *CG6646* and *CG1349* (referred to as *DJ-1A* and *DJ-1B*, respectively), which are homologous to human *DJ-1*. Sequence alignment shows that DJ-1A contains the three conserved amino acids proposed to form a putative catalytic triad in human DJ-1 (25), whereas DJ-1B lacks one of the three amino acids. This finding suggests that DJ-1A may be more closely related to human DJ-1. As a first step toward addressing the function of DJ-1A in *Drosophila*, we used the transgenic RNAi approach to knockdown DJ-1A expression (20). To confirm that the expression of *DJ-1A* dsRNA resulted in a down-regulation of endogenous *DJ-1A* transcripts, we used quantitative RT-PCR to measure *DJ-1A* mRNA levels after ubiquitous induction of DJ-1A RNAi. A dramatic reduction of *DJ-1A* mRNA was observed, whereas *DJ-1B* mRNA was relatively unchanged (Fig. 1*A*). We next tested the effect of RNAi on endogenous DJ-1 protein expression using DJ-1A- and DJ-1B-specific antibodies. As shown in Fig. 1*B*, ubiquitous DJ-1A RNAi resulted in a significant reduction of endogenous DJ-1A protein expression on Western blots. In contrast, the level of DJ-1B protein was relatively unaffected. Taken together, these results show that RNAi causes a specific knockdown of DJ-1A RNA and protein expression.

Targeted Inhibition of DJ-1A in the Eye Results in Photoreceptor Loss. We next analyzed the physiological consequence of inhibiting DJ-1A function. Ubiquitous expression of *DJ-1A* dsRNA with *actin-GAL4* or *daughterless (Da)*-GAL4 resulted in larval lethality. This finding suggests that DJ-1A is an essential gene in *Drosophila*. To circumvent the lethality problem, we used well characterized GAL4 drivers to inhibit DJ-1A expression in specific tissues and cell types and at different stages. Induction of DJ-1A RNAi in the developing eye using *GMR-GAL4* driver produced a rough eye phenotype (Fig. 1 *D* and *H*). *GMR-GAL4* directs gene expression in postmitotic cells posterior to the morphogenetic furrow and a small group of premitotic cells in the developing eye. Staining of eye sections revealed loss of photoreceptor neurons in some ommatidia (Fig. 1*J*), indicating that the rough eye phenotype is caused at least in part by photoreceptor cell loss. This RNAi effect is dosage-dependent, because increasing the copy number of *GAL4* and *UAS* transgenes caused a more severe degeneration of the eye (Fig. 1*K*). Several lines of evidence suggest that this eye phenotype is caused by specific inhibition of DJ-1A. First, overexpression of *white* or *dParkin* control dsRNAs using the same *GAL4* driver had no effect on eye morphology (data not shown), suggesting that the eye phenotype was not due to a nonspecific effect of dsRNA expression. Second, in a *DJ-1A* heterozygous genetic background, the eye phenotype was significantly enhanced (Fig. 1*F*), consistent with the RNAi effect being dosage dependent. Finally, we could rescue the RNAi phenotype with increased expression of *DJ-1A*. Given that the RNAi effect is dosage-dependent, we reasoned that, by raising the basal level of *DJ-1A* transcripts, the RNAi effect would be dampened. Indeed, coexpression of *UAS-DJ-1A* transgenes partially suppressed the eye degeneration phenotype induced by strong RNAi (Fig. 1, compare *M* with *K*). Coexpression of a human DJ-1 transgene could also partially rescue (Fig. 1, compare *N* with *K*), suggesting that human DJ-1 and fly DJ-1A may possess similar properties. In contrast, coexpression of a *GFP* transgene had no effect (Fig. 1, compare *L* with *K*), suggesting that the rescue is not due to titration of GAL4 by added expression of a *UAS*-transgene. We conclude that the abnormal eye phenotype is specifically caused by inhibition of DJ-1A expression.

Inhibition of _DJ-1A_ in Dopaminergic Neurons Leads to Decreases of TH Neuron Number and Brain DA Content. We next analyzed the effects of inhibiting DJ-1A function in dopaminergic neurons by

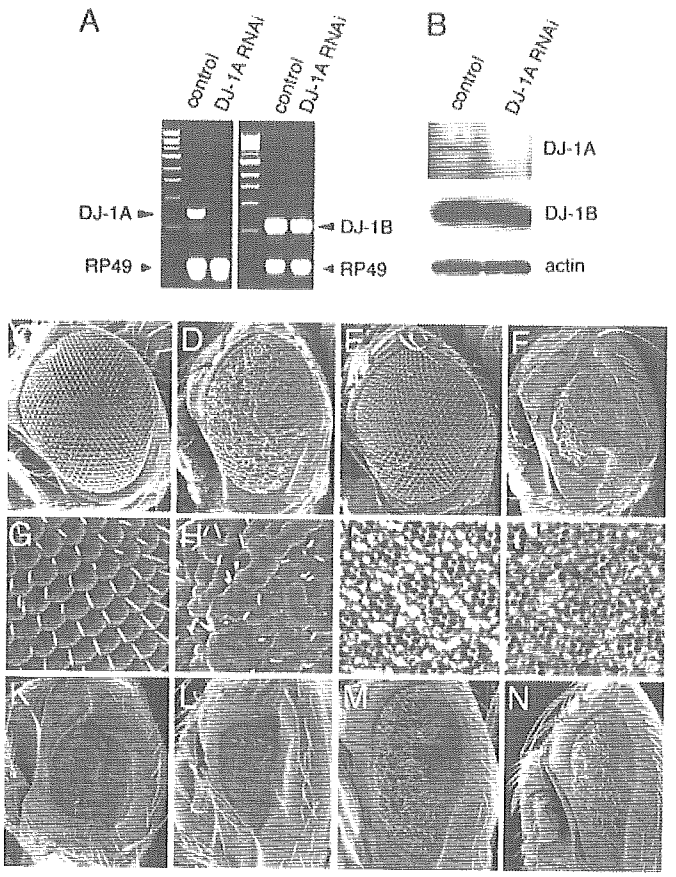

Fig. 1. Inhibition of *DJ-1A* expression by RNAi leads to photoreceptor neuron loss and eye degeneration. (*A*) Quantitative RT PCR analysis of *DJ-1A* mRNA level after RNAi. *DJ-1B* and *RP49* serve as controls. (*B*) Western blot analysis of DJ-1A protein level after RNAi. DJ-1B and actin serve as controls. (*C–H*) SEM images of *GMR-GAL4* (*C*), *GMR-GAL4 UAS-DJ-1A-RNAi* (*D*), *GMR-GAL4 Df(2R)CX1* (*E*), and *GMR-GAL4 UAS-DJ-1A-RNAi Df(2R)CX1* (*F*) eyes. *Df(2R)CX1* is a chromosomal deficiency that deletes *DJ-1A*. *G* and *H* are magnified views of *C* and *D*, respectively. (*I* and *J*) Staining of photoreceptor neurons in *GMR-GAL4* (*I*), and *GMR-GAL4 UAS-DJ-1A-RNAi* (*J*) eyes. Arrows in *J* mark ommatidia with photoreceptor loss. (*K–N*) Rescue of DJ-1A RNAi phenotypes by overexpressing *DJ-1A* or human *DJ-1*. All flies are homozygous for a recombinant *GMR-GAL4;UAS-DJ-1A-RNAi* chromosome and thus have a stronger phenotype than the one shown in *B*. In addition, the flies coexpress *UAS-GFP* (*L*), *UAS-DJ-1A* (*M*), *UAS-hDJ-1* (*N*), or no other transgene (*K*).

inducing RNAi with the *Ddc-GAL4* driver. We focused on the dopaminergic neurons in the dorsomedial clusters (DMC), which are known to be susceptible under disease conditions (26). Immunostaining of paraffin brain sections of *Ddc-GAL4 DJ-1A RNAi* flies revealed an age-dependent reduction in the number of TH neurons in the DMC. In 1-day-old flies, a normal complement of TH neurons (18) was present (Fig. 2*C*), but, in 35-day and older flies, only 10–12 of these neurons could be detected immunochemically (Fig. 2 *B* and *C*). Control flies showed no significant change in the number of these neurons during aging (Fig. 2 *A* and *C*). Induction of DJ-1A RNAi with another dopaminergic GAL4 driver, *TH-GAL4*, or the pan-neuronal *elav-GAL4* driver also resulted in reduction of TH neurons in the DM clusters (Fig. 2*C*).

To further confirm that loss of DJ-1A leads to dopaminergic dysfunction, we measured brain DA levels using head extracts prepared from control and *DJ-1A RNAi* flies. In newly eclosed flies, DA content was comparable between control and *RNAi* flies (Fig. 2*D*). However, 1 day after eclosion, *DJ-1A RNAi* flies showed significantly reduced DA level than control flies. At 4, 7, and 10 days of age, control and *DJ-1A RNAi* flies both showed age-dependent

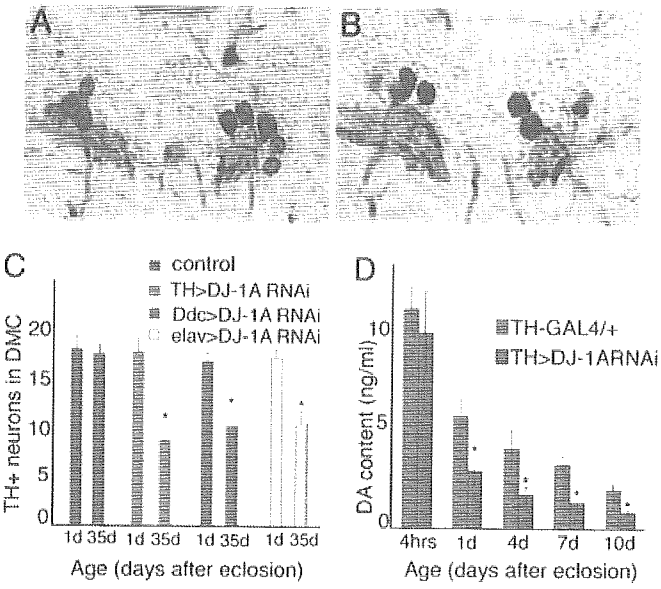

Fig. 2. Dopaminergic defects in *DJ-1A RNAi* flies. (*A* and *B*) TH immunostaining of DMC dopaminergic neurons in 35-day-old control *Ddc-GAL4* (*A*) and *Ddc-GAL4 DJ-1A RNAi* (*B*) male flies. Sections containing most of the DMC dopaminergic neurons are shown. (*C*) Quantification of TH neurons in the DMC of control flies and *DJ-1A RNAi* flies directed with *TH-GAL4*, *Ddc-GAL4*, or *elav-GAL4* drivers. The difference in cell count between 1-day-old and 35-day-old *DJ-1A RNAi* flies is significant. *, P 0.01 in Student's t test. (*D*) Quantification of head DA levels in *TH-GAL4* and *TH-GAL4 DJ-1A RNAi* flies. *, P 0.01 in Student's t test.

decline of DA, but *DJ-1A RNAi* flies consistently exhibited more reduction than the controls (Fig. 2*D*). Because a normal complement of TH dopaminergic neurons was present in 1-day old flies, the reduction of brain DA content at this early stage could not be attributed to neuronal loss. This result suggests that, in addition to promoting dopaminergic neuron survival, *Drosophila* DJ-1A may play an early role in regulating brain DA levels.

***DJ-1A RNAi* Flies Show Elevated ROS Accumulation and Hypersensitivity to Oxidative Stress.** We further characterized the *DJ-1A RNAi* animals to learn DJ-1A function *in vivo*. Human DJ-1 was previously found to respond to oxidative stress (8). This finding prompted us to analyze the response of *DJ-1A RNAi* flies under oxidative conditions. We used the *elav*-GAL4 driver to systematically induce DJ-1A RNAi in postmitotic neurons of transgenic flies and examined the response of these flies to treatment with exogenous H_2O_2. When treated with 1% H_2O_2, the time to reach 50% mortality was shortened by 27% in *DJ-1A RNAi* flies than control flies (Fig. 3*A*). This finding suggests that neuronal DJ-1A is important in fending off H_2O_2-induced lethality. To further confirm the sensitivity of *DJ-1A RNAi* flies to intracellular H_2O_2 levels, we treated DJ-1A RNAi flies with 3-AT, a known inhibitor of catalase, which converts H_2O_2 to H_2O. DJ-1A RNAi flies were found to be more sensitive to 3-AT treatment than the control flies (Fig. 3*B*). To test whether DJ-1A may be actively involved in ROS scavenging, we also overexpressed DJ-1A ubiquitously with the Da-GAL4 driver and observed that DJ-1A overexpression was sufficient to confer resistance against 3-AT treatment (Fig. 6, which is published as supporting information on the PNAS web site).

If DJ-1A normally plays a critical role in sensing cellular ROS levels and eliciting protective responses to remove these toxic agents, one would predict that inhibiting DJ-1A function would lead to elevated levels of endogenous ROS. We tested this possibility by staining cultured neurons with DCFH-DA, which is an indicator of hydroxyl free radicals. Compared with control neuronal culture,

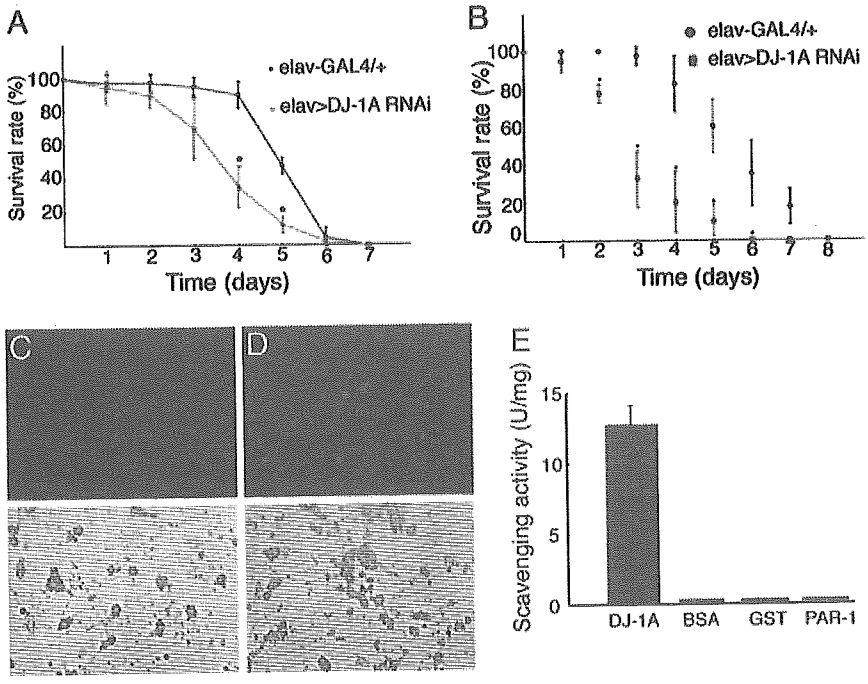

Fig. 3. DJ-1A RNAi leads to ROS accumulation and hypersensitivity to oxidative stress. (*A* and *B*) Comparison of survival curves of *elav-GAL4* flies with *elav-GAL4 DJ-1A RNAi* flies that are treated with 1% H2O2 (*A*) or 100 mM 3-AT (*B*). (*C* and *D*) DCFH-DA staining of cultured *Da-GAL4* (*C*) and *Da-GAL4 DJ-1A RNAi* (*D*) neurons. (*Upper*) Fluorescent DCFH-DA staining in green. (*Lower*) Black and white images of the neuronal culture being analyzed. (*E*) Recombinant DJ-1A protein exhibits detectable *in vitro* H_2O_2 scavenging activity, whereas the control proteins BSA, GST, and PAR-1 have no such activity.

which only showed weak ROS staining in a small percentage of neurons, *DJ-1A RNAi* neuronal culture had more neurons stained by this dye, and the staining intensity was much higher (Fig. 3, compare *D* with *C*).

Human DJ-1 protein was previously shown to be able to eliminate H2O2 *in vitro* by oxidizing itself at specific Cys residues (10, 27). To test whether *Drosophila* DJ-1A has similar H_2O_2 scavenging activity, we incubated bacterially expressed recombinant DJ-1A protein with H_2O_2 in test tubes and measured the conversion of H_2O_2. DJ-1A protein was found to have a specific activity in scavenging H_2O_2, whereas a control BSA protein has no such activity (Fig. 3*E*). This activity may not be simply attributed to nonspecific reaction of H_2O_2 with Cys residues, because the amino acid composition of BSA has a higher percentage of Cys residues than DJ-1A. Instead, this result indicates that DJ-1A may possess a specific activity in eliminating H_2O_2. In addition to BSA, which is normally resides in an extracellular environment, two intracellular proteins, GST and the Ser Thr protein kinase PAR-1, also showed no H_2O_2 scavenging activity. It should be noted that the H_2O_2 scavenging activity of DJ-1A was two orders of magnitude lower than that of catalase in the same assay (20 units mg vs. 2,300 units mg), suggesting that degrading H_2O_2 may not be the main function of DJ-1A.

Modulation of DJ-1A RNAi-Induced Cell Death by the PI3K Akt-Signaling Pathway. In an effort to understand how DJ-1A dysfunction leads to neuronal death, we tested possible genetic modification of DJ-1A RNAi-induced eye phenotypes by candidate genes and signaling pathways previously implicated in cell survival regulation. To see the genetic interaction more clearly, we used the weak RNAi phenotype induced by one copy each of the *GMR-GAL4* and *DJ-1A RNAi* transgenes to score for enhancement; the stronger RNAi phenotype induced by two copies of the *GMR-GAL4* and *DJ-1A RNAi* transgenes was used to score for suppression whenever possible.

The EGF receptor (EGFR) Ras1 mitogen-activated protein kinase (MAPK) signaling pathway has previously been shown to directly target the *Drosophila* proapoptotic gene *head involution defective* (*hid*) in the eye through MAPK-mediated phosphorylation and inactivation of HID (28). By using loss-of-function and gain-of-function alleles of *rolled* (*MAPK*) and loss-of-function alleles of *hid*, we did not detect clear genetic interaction with DJ-1A RNAi flies (data not shown). Similarly, we could not detect clear genetic interaction between DJ-1A RNAi and loss-of-function or overexpression alleles of genes in the JNK pathway, which has also been shown to induced cell death in the eye when activated (29).

In contrast, a clear genetic interaction was detected between DJ-1A and the *Drosophila* PI3K Akt pathway genes. A dramatic enhancement of DJ-1A RNAi-induced eye degeneration was observed when *PTEN* was coexpressed with the DJ-1A RNAi transgene (Fig. 4*D*). The resulting fly eyes were dramatically reduced in size, with collapsed and fused ommatidia and necrotic spots, which were not present in DJ-1A RNAi only flies. Staining of photoreceptor neurons revealed a near complete loss of photoreceptor neurons in *PTEN* coexpression fly eyes (data not shown). Overexpression of this *UAS-PTEN* transgene alone with *GMR-GAL4* driver had little effect on the regular organization of the ommatidia and photoreceptor number per ommatidium, although the overall size of the eye was moderately reduced (Fig. 4*L*). When we tested with a mutant form of human PTEN that contains an inactivating C124S mutation (18), no effect on DJ-1A RNAi phenotype was observed (data not shown). Similar to the effect of *Drosophila PTEN*, an enhancement of the DJ-1A RNAi phenotype was observed when a dominant-negative (DN) form of PI3K catalytic subunit *Dp110* (*PI3K DN*) was coexpressed (17) (Fig. 4*C*), although expression of this *PI3K DN* transgene alone had little effect on eye morphology (Fig. 4*K*).

A clear suppression of DJ-1A RNAi phenotype was observed when the wild-type form of PI3K catalytic subunit *Dp110* was coexpressed. The eyes were restored to normal size, and the organization of the ommatidia was significantly improved (Fig. 4*B*). Overexpression of a *UAS-Akt* transgene had similar effect as *PI3K* in suppressing DJ-1A RNAi-induced toxicity in the eye (Fig. 4*A*), consistent with Akt PKB being a key downstream effecter component in the PI3K-signaling pathway (16).

Given the known pleiotropic function of the PI3K-signaling pathway in regulating cell size and cell number in *Drosophila* and its potential role in regulating cell survival, we next tested the effect of manipulating PI3K pathway gene activity on an eye degeneration phenotype caused by a different mechanism. Overexpression of human *tau* in the fly eye also led to a reduction in eye size and loss of photoreceptor neurons (19, 22). In contrast to the *DJ-1A RNAi*

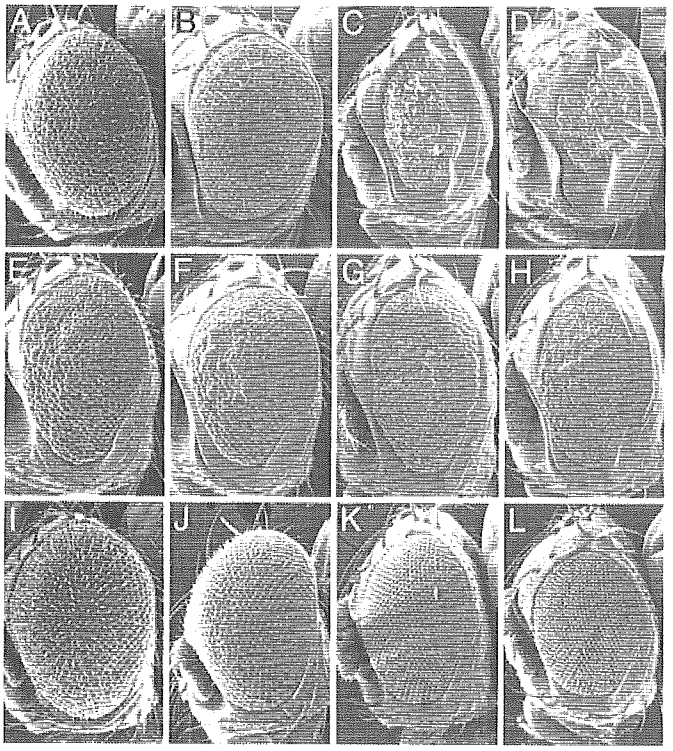

Fig. 4. Modification of DJ-1A RNAi phenotypes by altered expression of genes in the PI3K Akt pathway. (*A–D*) SEM eye images of DJ-1A RNAi flies coexpressing *UAS-Akt* (*A*), *UAS-PI3K Dp110* (*B*), *UAS-PI3K Dp110DN* (*C*), or *UAS-PTEN* (*D*). (*E–H*) SEM eye images of human tauV337M transgenic flies coexpressing *UAS-GFP* (*E*), *UAS-PI3K Dp110* (*F*), *UAS-PI3K Dp110DN* (*G*), or *UAS-PTEN* (*H*). (*I–L*) SEM eye images of flies expressing *UAS-Akt* (*I*), *UAS-PI3K Dp110* (*J*), *UAS-PI3K Dp110DN* (*K*), or *UAS-PTEN* (*L*) transgenes alone. *GMR-GAL4* was used to direct *UAS* transgene expression in all panels.

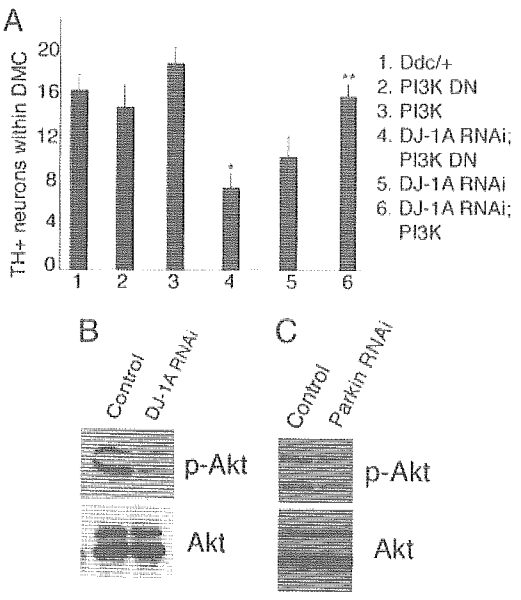

Fig. 5. Modification of DJ-1A RNAi-induced dopaminergic phenotype by altered expression of *PI3K Akt* pathway genes and Western blot analysis showing reduced Akt phosphorylation after DJ-1A or Parkin down-regulation. (*A*) Quantification of TH DA neurons in the DMC of *Ddc-GAL4* control flies, *DJ-1A RNAi* flies, *PI3K* or *PI3K DN* single overexpression flies, and *DJ-1A RNAi* flies coexpressing *PI3K* or *PI3K DN* transgenes. *, P 0.01 in Student's t test. *Ddc-GAL4* was used to direct transgene expression. (*B* and *C*) Western blot analysis of fly head extracts prepared from *Da-GAL4* and *Da-GAL4 DJ-1A RNAi* (*B*) or *Da-GAL4* and *Da-GAL4 dParkin RNAi* (*C*) genotyped flies. Blots were probed with anti-phospho-Akt and anti-Akt antibodies, respectively.

situation, coexpression of wild-type *PI3K*, *PI3K DN*, or *PTEN* showed little effect on human tau-induced toxicity in the eye (Fig. 4, compare *F*, *G*, and *H*, respectively, with *E*). The genetic interaction between DJ-1A and PI3K pathway genes in the eye thus seems to be rather specific.

We next tested the effects of modulating PI3K signaling on the dopaminergic degeneration phenotype induced by DJ-1A RNAi. Coexpression of PI3K completely suppressed the reduction of TH DA neuron phenotype induced by DJ-1A RNAi. The number of DA neurons in the DMCs was maintained at the wild-type level in all of the transgenic flies and at all ages examined (Fig. 5*A*), indicating that coexpression of PI3K blocked DJ-1A RNAi-induced age-dependent dopaminergic degeneration. Conversely, coexpression of PI3K DN showed a statistically significant enhancement of DJ-1A RNAi toxicity in dopaminergic neurons (Fig. 5*A*).

We next examined the effect of PI3K signaling on DJ-1A RNAi-induced ROS accumulation. We found that, in adult fly brain, induction of DJ-1A RNAi within dopaminergic neurons led to an elevation of ROS levels, consistent with neuronal culture studies described earlier (Fig. 7*A*, which is published as supporting information on the PNAS web site). Inhibition of PI3K signaling in these neurons by means of overexpression of PI3K DN also led to elevation of ROS levels (Fig. 7*B*), whereas flies overexpressing wild-type PI3K showed basal ROS levels (Fig. 7*C*). Strikingly, in DJ-1A RNAi flies coexpressing PI3K, cellular ROS levels are reduced to baseline levels as in wild-type controls (Fig. 7*G*). Together, these results indicate that PI3K signaling specifically suppresses DJ-1A RNAi-induced neurotoxicity and that this suppression is correlated with a reduction of cellular ROS levels.

DJ-1A RNAi Flies and Parkin Mutant Flies Exhibit Impaired PI3K Akt Signaling. The fact that increased PI3K Akt signaling specifically suppressed DJ-1A RNAi-induced cell death suggests that the cell death in DJ-1A RNAi animals may be caused by a reduction of PI3K Akt signaling. To test this possibility, we examined the phosphorylation status of Akt, an indicator of PI3K Akt signaling, in DJ-1A RNAi animals. Head extracts from *Da-GAL4* and *Da-GAL4 DJ-1A RNAi* animals were analyzed by Western blot analysis by using anti-phospho-Akt and anti-Akt antibodies. As shown in Fig. 5*B*, although the level of total Akt protein was comparable between control and DJ-1A RNAi fly heads, the amount of phospho-Akt was significantly reduced in *DJ-1A RNAi* animals. This result indicates that DJ-1A down-regulation leads to hypophosphorylation of Akt and impairment of PI3K Akt signaling in the fly brain. To test whether impairment of PI3 Akt signaling is a general feature of PD models, we analyzed the *Drosophila parkin* model. As shown in Fig. 5*C*, inhibition of Parkin function also led to a reduction of phospho-Akt levels. These results implicate reduced PI3K Akt signaling as a common molecular event in the pathogenic cascade of PD.

Discussion

Loss-of-function mutations in human DJ-1 are linked to familial Parkinson's disease. The exact molecular function of DJ-1 that is relevant to disease pathogenesis is not well understood. Our results suggest that *Drosophila* DJ-1A plays an important role in cellular ROS homeostasis and protection against oxidative stress. This conclusion is consistent with previous studies in mammalian cell culture and DJ-1 knockout mice (13, 27, 30). Human DJ-1 was found to have H_2O_2-scavenging activity *in vitro*. (10) (27). Our analysis of *Drosophila* DJ-1A protein supported this notion. However, the H_2O_2-converting activity of DJ-1A is rather low compared with catalase, suggesting that the main molecular function of DJ-1 may not be limited to degrading H_2O_2. It is possible that the ability

to react with H_2O_2 by means of oxidation-sensitive Cys residues may allow DJ-1 to act as a "sensor" of cellular ROS levels, and the oxidized DJ-1 may subsequently acquire a new function to defend against ROS-induced cellular damages. This result would be analogous to the switch of two yeast peroxiredoxins from peroxidase to molecular chaperone under oxidative stress (31). The recent description of human DJ-1 gaining molecular chaperone activity *in vitro* under oxidative conditions is consistent with this model (32).

To understand the cellular processes that mediated DJ-1A dysfunction-induced cell death, we performed genetic interaction studies with genes and signaling pathways that are involved in cell survival and identified components of the PI3K PTEN Akt pathway as modulators of DJ-1 RNAi-induced cell death phenotype. Increase of PI3K Akt-signaling capacity showed suppression, whereas decreased PI3K Akt signaling enhanced DJ-1A RNAi phenotypes. The effects of modulating PI3K Akt signaling on DJ-1A RNAi-induced toxicity hold true in both photoreceptor neurons in the retina and dopaminergic neurons in the central brain, suggesting that the connection between DJ-1 and PI3K Akt signaling is a general phenomenon. The finding that DJ-1A RNAi animals showed decreased phosphorylation of Akt indicate that DJ-1 is a regulator of PI3K Akt signaling. A recent study by Kim *et al.* (15) identified DJ-1A as a suppressor of PTEN function in the fly eye, and the authors further extended this finding to mammalian cells and showed that DJ-1 knockdown by small interfering RNA results in decreased phosphorylation of PKB Akt, whereas DJ-1 overexpression leads to PKB Akt hyperphosphorylation and increased cell survival. This finding led to the proposal that DJ-1 acts as a novel regulator of PTEN. Our genetic and biochemical studies are consistent with this notion. It is not clear at this point how DJ-1A and the PI3K PTEN Akt-signaling pathway may interact. It is possible that the function of DJ-1 in regulating cellular ROS homeostasis or as a redox-sensitive molecular chaperone may facilitate PI3K PTEN Akt signaling, because many signal transduction pathways are known to be sensitive to cellular ROS levels or require chaperone activities (33, 34), and modulation of PTEN activity by ROS has been reported before (35). Alternatively, the genetic interaction between DJ-1A and PI3K-signaling pathway may be mediated by a direct role of PI3K signaling in cellular defense against ROS accumulation and related damages. Our data are consistent with both possibilities. Given that hyperactivation of DJ-1 could be oncogenic, whereas its deficiency leads to neuronal dysfunction and degeneration, future studies aimed at understanding the mechanisms by which DJ-1 and PI3K PTEN Akt pathway interact will have far-reaching implications for understanding disease mechanisms and developing therapeutic strategies.

Oxidative stress and mitochondrial dysfunction are being increasingly recognized as common pathological features of neurodegenerative diseases including PD and Alzheimer's disease (2, 36). Previous genetic studies in *Drosophila* and mice have implicated Parkin, an E3 ubiquitin ligase associated with autosomal recessive juvenile parkinsonism, in these processes (37–40). In flies and mice, *parkin* mutants show defects in mitochondrial function and oxidative stress response. Like DJ-1, loss of *Drosophila* Parkin function also affects the viability of mutant animals. This result contrasts with the situation in mammals where loss of DJ-1 or Parkin is nonlethal. The differential effects on the viability of humans and flies are probably caused by fundamental differences in the antioxidant defense systems of these two species (41). The exact cellular mechanism by which Parkin dysfunction leads to susceptibility to oxidative stress and cell death remains to be established. Our finding that, similar to DJ-1A inactivation, inhibition of *parkin* also leads to impairment of PI3K Akt signaling implicates these two genes in a common pathway that promotes neuronal survival. We speculate that impairment of PI3K Akt signaling may be a common feature of familial as well as sporadic PD cases and that manipulation of this signaling pathway may provide a rational strategy for the therapeutic intervention of PD.

We are grateful to Drs. Morris Birnbaum (University of Pennsylvania, Philadelphia), Mel Feany (Harvard University, Boston), Ernst Hafen (University of Zurich, Zurich), Raj Sohal (University of Southern California, Los Angeles), Bertrand Mollereau (The Rockefeller University, New York), Hermann Steller (The Rockefeller University), Tian Xu (Yale University, New Haven, CT), and the Bloomington *Drosophila* Stock Center for fly stocks; Dr. Kazuaki Yoshikawa for his generous support; the Center for Research and Education of Osaka University School of Medicine for help with SEM and eye sectioning; Dr. Su Guo for reading the manuscripts; Dr. Ting-ting Huang for help with H_2O_2 assay; and Dr. Kyung-Tai Min for communicating unpublished results. Special thanks go to Jennifer Quach and Yali Zhang for excellent technical support and members of the B.L. laboratory for discussions. This work was supported by the McKnight, Beckman, and Sloan Foundations (to B.L.).

1. Dunnett, S. B. & Bjorklund, A. (1999) *Nature* **399**, A32–A39.
2. Dawson, T. M. & Dawson, V. L. (2003) *Science* **302**, 819–822.
3. Shen, J. & Cookson, M. R. (2004) *Neuron* **43**, 301–304.
4. Nagakubo, D., Taira, T., Kitaura, H., Ikeda, M., Tamai, K., Iguchi-Ariga, S. M. & Ariga, H. (1997) *Biochem. Biophys. Res. Commun.* **231**, 509–513.
5. Hod, Y., Pentyala, S. N., Whyard, T. C. & El-Maghrabi, M. R. (1999) *J. Cell Biochem.* **72**, 435–444.
6. Takahashi, K., Taira, T., Niki, T., Seino, C., Iguchi-Ariga, S. M. & Ariga, H. (2001) *J. Biol. Chem.* **276**, 37556–37563.
7. Canet-Aviles, R. M., Wilson, M. A., Miller, D. W., Ahmad, R., McLendon, C., Bandyopadhyay, S., Baptista, M. J., Ringe, D., Petsko, G. A. & Cookson, M. R. (2004) *Proc. Natl. Acad. Sci. USA* **101**, 9103–9108.
8. Mitsumoto, A. & Nakagawa, Y. (2001) *Free Radical Res.* **35**, 885–893.
9. Mitsumoto, A., Nakagawa, Y., Takeuchi, A., Okawa, K., Iwamatsu, A. & Takanezawa, Y. (2001) *Free Radical Res.* **35**, 301–310.
10. Kinumi, T., Kimata, J., Taira, T., Ariga, H. & Niki, E. (2004) *Biochem. Biophys. Res. Commun.* **317**, 722–728.
11. Yokota, T., Sugawara, K., Ito, K., Takahashi, R., Ariga, H. & Mizusawa, H. (2003) *Biochem. Biophys. Res. Commun.* **312**, 1342–1348.
12. Goldberg, M. S., Pisani, A., Haburcak, M., Vortherms, T. A., Kitada, T., Costa, C., Tong, Y., Martella, G., Tscherter, A., Martins, A., *et al.* (2005) *Neuron* **45**, 489–496.
13. Kim, R. H., Smith, P. D., Aleyasin, H., Hayley, S., Mount, M. P., Pownall, S., Wakeham, A., You-Ten, A. J., Kalia, S. K., Horne, P., *et al.* (2005) *Proc. Natl. Acad. Sci. USA* **102**, 5215–5220.
14. Chen, L., Cagniard, B., Mathews, T., Jones, S., Koh, H. C., Ding, Y., Carvey, P. M., Ling, Z., Kang, U. J. & Zhuang, X. (2005) *J. Biol. Chem.* **280**, 21418–21426.
15. Kim, R. H., Peters, M., Jang, Y., Shi, W., Pintilie, M., Fletcher, G. C., DeLuca, C., Liepa, J., Zhou, L., Snow, B., *et al.* (2005) *Cancer Cell* **7**, 263–273.
16. Verdu, J., Buratovich, M. A., Wilder, E. L. & Birnbaum, M. J. (1999) *Nat. Cell Biol.* **1**, 500–506.
17. Leevers, S. J., Weinkove, D., MacDougall, L. K., Hafen, E. & Waterfield, M. D. (1996) *EMBO J.* **15**, 6584–6594.
18. Huang, H., Potter, C. J., Tao, W., Li, D. M., Brogiolo, W., Hafen, E., Sun, H. & Xu, T. (1999) *Development (Cambridge, U.K.)* **126**, 5365–5372.
19. Wittmann, C. W., Wszolek, M. F., Shulman, J. M., Salvaterra, P. M., Lewis, J., Hutton, M. & Feany, M. B. (2001) *Science* **293**, 711–714.
20. Kalidas, S. & Smith, D. P. (2002) *Neuron* **33**, 177–184.
21. Yang, Y., Nishimura, I., Imai, Y., Takahashi, R. & Lu, B. (2003) *Neuron* **37**, 911–924.
22. Nishimura, I., Yang, Y. & Lu, B. (2004) *Cell* **116**, 671–682.
23. Ito, S., Kato, T. & Fujita, K. (1988) *Biochem. Pharmacol.* **37**, 1707–1710.
24. Beal, M. F., Kowall, N. W., Swartz, K. J. & Ferrante, R. J. (1990) *Neurosci. Lett.* **108**, 36–42.
25. Tao, X. & Tong, L. (2003) *J. Biol. Chem.* **278**, 31372–31379.
26. Feany, M. B. & Bender, W. W. (2000) *Nature* **404**, 394–398.
27. Taira, T., Saito, Y., Niki, T., Iguchi-Ariga, S. M., Takahashi, K. & Ariga, H. (2004) *EMBO Rep.* **5**, 213–218.
28. Bergmann, A., Agapite, J., McCall, K. & Steller, H. (1998) *Cell* **95**, 331–341.
29. Kuranaga, E., Kanuka, H., Igaki, T., Sawamoto, K., Ichijo, H., Okano, H. & Miura, M. (2002) *Nat. Cell Biol.* **4**, 705–710.
30. Martinat, C., Shendelman, S., Jonason, A., Leete, T., Beal, M. F., Yang, L., Floss, T. & Abeliovich, A. (2004) *PloS Biol.* **2**, e327.
31. Jang, H. H., Lee, K. O., Chi, Y. H., Jung, B. G., Park, S. K., Park, J. H., Lee, J. R., Lee, S. S., Moon, J. C., Yun, J. W., *et al.* (2004) *Cell* **117**, 625–635.
32. Shendelman, S., Jonason, A., Martinat, C., Leete, T. & Abeliovich, A. (2004) *PLoS Biol.* **2**, e362.
33. Shibata, Y., Branicky, R., Landaverde, I. O. & Hekimi, S. (2003) *Science* **302**, 1779–1782.
34. Morey, M., Serras, F., Baguna, J., Hafen, E. & Corominas, M. (2001) *Dev. Biol.* **238**, 145–156.
35. Leslie, N. R., Bennett, D., Lindsay, Y. E., Stewart, H., Gray, A. & Downes, C. P. (2003) *EMBO J.* **22**, 5501–5510.
36. Albers, D. S. & Beal, M. F. (2000) *J. Neural Transm.* **59**, Suppl., 133–154.
37. Kitada, T., Asakawa, S., Hattori, N., Matsumine, H., Yamamura, Y., Minoshima, S., Yokochi, M., Mizuno, Y. & Shimizu, N. (1998) *Nature* **392**, 605–608.
38. Greene, J. C., Whitworth, A. J., Kuo, I., Andrews, L. A., Feany, M. B. & Pallanck, L. J. (2003) *Proc. Natl. Acad. Sci. USA* **100**, 4078–4083.
39. Pesah, Y., Pham, T., Burgess, H., Middlebrooks, B., Verstreken, P., Zhou, Y., Harding, M., Bellen, H. & Mardon, G. (2004) *Development (Cambridge, U.K.)* **131**, 2183–2194.
40. Palacino, J. J., Sagi, D., Goldberg, M. S., Krauss, S., Motz, C., Klose, J. & Shen, J. (2004) *J. Biol. Chem.* **279**, 18614–18622.
41. Kanzok, S. M., Fechner, A., Bauer, H., Ulschmid, J. K., Muller, H. M., Botella-Munoz, J., Schneuwly, S., Schirmer, R. & Becker, K. (2001) *Science* **291**, 643–646.

nature neuroscience

Chromogranin-mediated secretion of mutant superoxide dismutase proteins linked to amyotrophic lateral sclerosis

Makoto Urushitani[1], Attila Sik[2], Takashi Sakurai[3], Nobuyuki Nukina[3], Ryosuke Takahashi[4] & Jean-Pierre Julien[1]

Here we report that chromogranins, components of neurosecretory vesicles, interact with mutant forms of superoxide dismutase (SOD1) that are linked to amyotrophic lateral sclerosis (ALS), but not with wild-type SOD1. This interaction was confirmed by yeast two-hybrid screen and by co-immunoprecipitation assays using either lysates from Neuro2a cells coexpressing chromogranins and SOD1 mutants or lysates from spinal cord of ALS mice. Confocal and immunoelectron microscopy revealed a partial colocalization of mutant SOD1 with chromogranins in spinal cord of ALS mice. Mutant SOD1 was also found in immuno-isolated trans-Golgi network and in microsome preparations, suggesting that it can be secreted. Indeed we report evidence that chromogranins may act as chaperone-like proteins to promote secretion of SOD1 mutants. From these results, and our finding that extracellular mutant SOD1 can trigger microgliosis and neuronal death, we propose a new ALS pathogenic model based on the toxicity of secreted SOD1 mutants.

ALS is a progressive adult-onset neurodegenerative disorder that affects primarily motor neurons in the brain and spinal cord. The disease typically begins locally and spreads, leading to paralysis and death within 3–5 years. Approximately 10% of ALS cases are familial and 90% are sporadic. Mutations in the genes encoding SOD1 (ref. 1) are involved in 20% of familial ALS cases.

Despite a decade of investigation on familial ALS caused by missense mutations in the *SOD1* gene, the mechanism of toxicity to motor neurons has remained elusive. Transgenic mice expressing mutant forms of SOD1 develop motor neuron disease resembling ALS through a gain of unidentified deleterious properties[2]. Eliminating the copper chaperone for SOD1 does not diminish the toxicity of mutant SOD1 in mice[3], and mutations that disrupt the copper-binding site of mutant SOD1 do not suppress toxicity[4]. Thus, it is now thought that the toxicity of mutant SOD1 is not related to aberrant copper-mediated catalysis but rather to the propensity of the abnormal protein to aggregate, a phenomenon common to many neurodegenerative diseases[5,6]. Cell culture studies have shown that the mutant SOD1 proteins induce oxidative stress[7,8], form aggregates[9,10] and impair proteasomal function[11].

Notably, recent lines of evidence indicate that the toxicity of SOD1 mutants is non-cell-autonomous. The neuron-specific expression of mutant SOD1 does not provoke motor neuron disease[12,13]. Moreover, chimeric mouse studies with SOD1 mutants have demonstrated that neurodegeneration is delayed or eliminated when motor neurons expressing mutant SOD1 are surrounded by healthy wild-type cells[14]. Moreover, these studies show evidence of damage to wild-type motor neurons by surrounding cells expressing mutant SOD1. Such results emphasize the importance of a motor neuron milieu, but the mechanism by which the toxicity of mutant SOD1 may be transferred from one cell to another is still unclear[14].

So far, proteins known to interact with mutant forms of SOD1 but not with wild-type SOD1 have been implicated in protein refolding or proteasomal degradation (for example, heat-shock proteins Hsp40, Hsp/Hsc70 (refs. 15,16) and CHIP[16]). To search for more proteins that interact with mutant SOD1, we performed yeast two-hybrid screening of a cDNA library from the total spinal cord of presymptomatic transgenic mice expressing the G93A SOD1 mutation (in which a glycine residue is replaced by an alanine residue). We discovered that chromogranins are interacting partners with mutant forms of SOD1, but not wild-type SOD1. The chromogranins, namely chromogranin-A (CgA) and chromogranin-B (CgB), are soluble, acidic glycophosphoproteins and are major constituents of secretory large dense-core vesicles (LDCV) in neurons and endocrine cells. LDCV store neuropeptides and hormones and show regulated exocytosis upon appropriate cellular stimulation[17]. Chromogranins are transported in the trans-Golgi network (TGN) and translocate at the periphery in an actin-dependent manner during their maturation process[18]. Although the physiological functions of chromogranins are still unclear, previous reports have shown that their proteolytic products function as antibiotics, regulators of hormone release, controllers of intracellular Ca^{2+} concentration and protein sorting machineries[17]. The role of chromogranins in neurons is unknown. Both CgA and CgB proteins are transported in the rat sciatic

[1]Department of Anatomy and Physiology, Laval University, Centre de Recherche du Centre Hospitalier de l' Université Laval, 2705 boulevard Laurier, Sainte-Foy, Quebec G1V 4G2, Canada. [2]Department of Psychiatry, Centre de Recherche Université Laval Robert-Giffard, 2601 de la Canardiere, Quebec, Quebec G1J 2G3, Canada. [3]Laboratory for Structural Neuropathology and [4]Motor System Neurodegeneration, RIKEN Brain Science Institute, 2-1 Hirosawa, Wako, Saitama, 351-0198, Japan. Correspondence should be addressed to J.-P.J. (jean-pierre.julien@crchul.ulaval.ca).

Received 15 September; accepted 26 October; published online 20 December 2005; doi:10.1038/nn1603

nerve[19] and CgA is found in motor endplates in the diaphragm[20], suggesting a possible role in neurotransmission.

Previous evidence indicates that chromogranins are involved in neurodegenerative diseases. Immunohistochemical studies have revealed the presence of CgA or CgB in neuritic senile plaques of Alzheimer brains[21] and in prion protein deposits of Creutzfeldt-Jacob disease brains[22]. The staining pattern of CgA is also altered in motor neurons of people with sporadic ALS[23]. Importantly, there is evidence that CgA can activate microglia to produce various pro-inflammatory molecules such as tumor necrosis factor-alpha (TNF-α), nitric oxide and potential neurotoxins including glutamate and cathepsin B[24–26].

Here we report that CgA and CgB, which are abundant proteins in motor neurons and interneurons, may act as chaperone-like proteins to

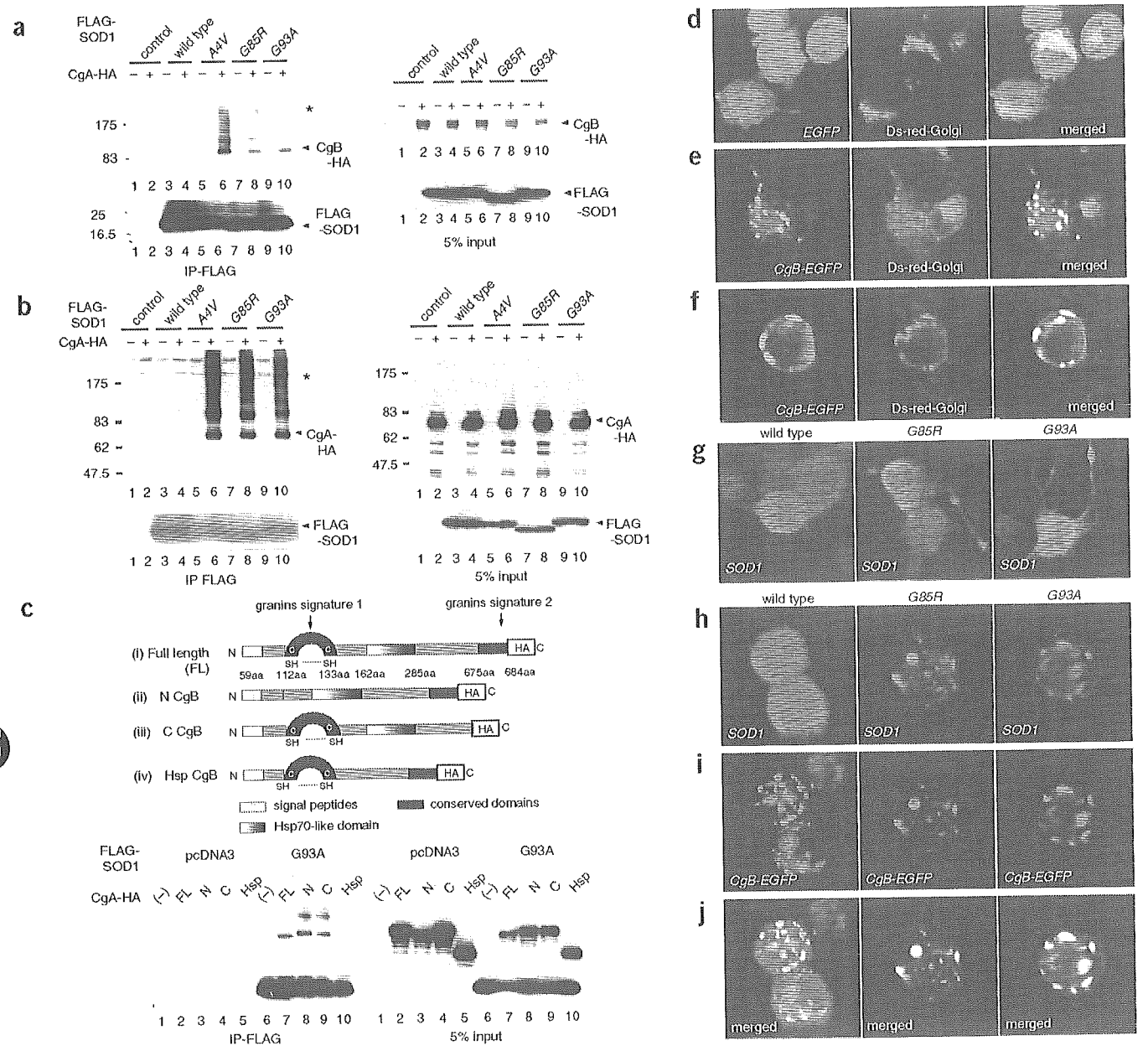

Figure 1 Selective interactions of chromogranins with mutant SOD1 species but not with wild-type SOD1. (**a**,**b**) Chromogranins interact with mutant SOD1 in cultured cells. Neuro2a cells were transiently transfected with FLAG-tagged human *SOD1* (wild-type, A4V, G85R or G93A) and HA-tagged mouse CgB (**a**) or CgA (**b**). Immunoprecipitates with anti-FLAG affinity gel (IP-FLAG) and total cell lysates (5% input) were analyzed by western blotting using antibodies to SOD1 or HA. Note that both CgB and CgA immunoprecipitated with mutant SOD1 to yield high molecular weight species (asterisk). (**c**) An Hsp70-like domain in CgB interacts with mutant SOD1. Schematic representation of full-length (FL) or deletion mutants (N terminus (ΔN), C terminus (ΔC) or Hsp70-like domain (ΔHsp)) of CgB (top). Total cell lysates and immunoprecipitates from Neuro2a cells transfected with *FLAG-SOD1* or full-length *CgB* (FL) or its deletion mutants (ΔN, ΔC, ΔHsp) were analyzed by western blotting using the same antibodies (bottom). (**d–f**) Localization of CgB in the TGN of transfected Neuro2a cells. Images show live cells from confocal laser microscope of Neuro2a cells transfected with a plasmid encoding Ds-Red and a Golgi marker (*Ds-Red-Golgi*, middle) and EGFP (**d**) or EGFP-fused CgB (*CgB-EGFP*, **e** and **f**). (**g–j**) Overexpressed SOD1 mutants localized with CgB in the TGN of Neuro2a cells. Neuro2a cells were transiently transfected with human SOD1 (wild-type, G85R and G93A) together with (**i–k**) or without (**h**) CgB-EGFP, and analyzed by immunocytochemistry using mouse monoclonal anti-SOD1.

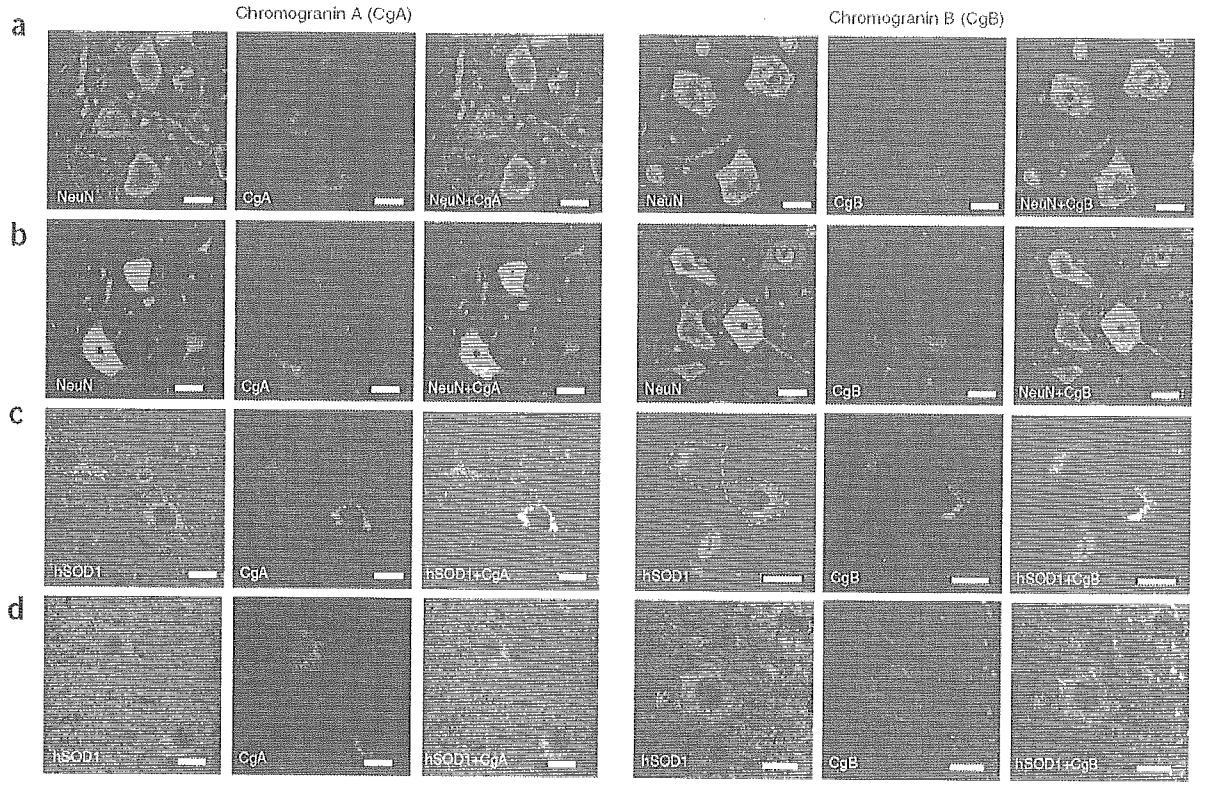

Figure 2 Expression pattern of chromogranins in *SOD1* transgenic mice. We used the lumbar spinal cords from (**a**) nontransgenic littermates, (**b**,**c**) transgenic mice at 7 months of age and (**d**) transgenic mice at 9 months of age. The transgenic mice expressed either G37R *SOD1* (**b**,**c**) or wild-type *SOD1* (**d**). The following combinations of antibody stains were used: (**a**,**b**) mouse monoclonal anti-NeuN plus rabbit polyclonal anti-CgA (left) or anti-CgB (right); (**c**,**d**) sheep polyclonal antibody specific to human SOD1 plus anti-CgA (left) or anti-CgB (right). In **c**, the dotted lines demarcate the cell body of motor neurons. Scale bars, 50 μm.

promote secretion of misfolded SOD1 mutants. Moreover, our results demonstrate that extracellular mutant SOD1 can induce microgliosis and motor neuron death, suggesting that the chromogranin-mediated secretion of mutant SOD1 proteins could be a pathogenic mechanism in ALS. This idea is consistent with findings that the disease is not strictly autonomous to motor neurons and that toxicity is transferable from one cell to another.

RESULTS

Interaction of CgA and CgB with mutant SOD1 in cultured cells

To identify new proteins that interact with mutant SOD1, we used a yeast two-hybrid approach to screen a cDNA library from the spinal cord of pre-symptomatic mice transgenic for human G93A *SOD1*, using monomeric LexA-human G93A SOD1 as bait. As expected, the majority of the 250 surviving clones expressed human SOD1 that can dimerize with the bait. However, we obtained one clone whose sequence corresponded to a partial mouse CgB sequence encoding 76 amino acids. A full-length mouse CgB clone was then isolated from a brain cDNA library of C57Bl/6 mice and used as bait in the yeast two-hybrid system to confirm a specific interaction of CgB with mutant SOD1, but not with wild-type SOD1 (data not shown). To further investigate the interaction of CgB with mutant forms of SOD1 in a mammalian cell system, we carried out transient coexpression assays with Neuro2a cells using plasmid vectors coding for CgB tagged with hemagglutinin (HA) at the carboxy (C) terminus and for various human SOD1 species tagged with FLAG at the amino (N) terminus. We tested various SOD1 mutants, including the A4V, G85R and G93A mutants, to confirm that chromogranins interact with misfolded SOD1 mutants in general, not just the G93A mutant. As shown in pull-down assays (**Fig. 1a**), CgB was co-immunoprecipitated with mutant forms of SOD1, but not with wild-type SOD1. Pull-down assays revealed that CgA, another member of the mouse chromogranin family, also associated with SOD1 mutants but not with wild-type SOD1 (**Fig. 1b**). Similar results were obtained with human chromogranins (data not shown).

CgA and CgB share two conserved domains near their N and C termini, named the granin domains. The N-terminal granin domain is implicated in a sorting mechanism[27], whereas the C-terminal granin domain is necessary for dimerization or tetramerization of chromogranins[28]. To determine the CgB region responsible for interaction with mutant SOD1, we constructed expression plasmids for CgB mutants lacking specific domains and transiently expressed them together with mutant SOD1 into Neuro2a cells (**Fig. 1c**, top). An immunoprecipitation experiment showed that CgB mutants with deleted granin domains (ΔN or ΔC) were still able to interact with mutant SOD1 (**Fig. 1c**, bottom). A search for sequence homologies revealed that both CgB and CgA contain internal sequences with homologies to the substrate-binding site of mammalian Hsp70 (**Supplementary Fig. 1** online). A CgB mutant lacking this internal region (ΔHsp) did not bind mutant SOD1, as determined by the pull-down assay (**Fig. 1c**). The presence of an Hsp70-like domain offers a reasonable explanation for the specific binding of chromogranins to misfolded SOD1 mutants and not to wild-type SOD1.

Confocal microscopy of transfected Neuro2a cells provided further evidence of interactions between SOD1 mutants and chromogranins. Transfection of a construct encoding CgB fused at the C terminus to

enhanced green fluorescent protein (EGFP) (*CgB-EGFP*) into Neuro2a cells showed CgB accumulation in the TGN, as indicated by colocalization with Ds-Red fused to the Golgi-targeting human β1,4-galactoysl-transferase (Ds-Red-Golgi) (**Fig. 1d–f**). Unlike chromogranins, SOD1 is a cytosolic protein without signal peptide and it is synthesized in free ribosomes. As expected, wild-type SOD1 yielded a cytosolic distribution when overexpressed in Neuro2a cells, and the expression of CgB had no effect on its distribution (**Fig. 1g–j**, left). In contrast, the subcellular distribution of mutant SOD1 species (G85R or G93A) was altered by the overexpression of CgB. A total colocalization of mutant SOD1 with CgB was observed in roughly 10% of doubly transfected Neuro2a cells (**Fig. 1g–j**, middle and right). These results indicate that CgB can influence the subcellular distribution of SOD1 mutants under the condition of overexpression in cultured cells.

Colocalization of mutant SOD1 and CgA/B *in vivo*

We confirmed by *in situ* hybridization that CgA and CgB are expressed throughout the gray matter of spinal cord in mice, in motor neurons, interneurons and dorsal neurons. Immunohistochemistry showed that both CgA and CgB are more predominantly detected in dorsal neurons and interneurons than in motor neurons (**Supplementary Fig. 2** online), which is consistent with previous reports[29,30].

Immunofluorescence microscopy showed that CgA and CgB are located in perinuclear vesicles in the spinal motor neurons of normal mice stained by anti-NeuN antibody (**Fig. 2a**). In presymptomatic *G37R SOD1* mice (7 months old), perinuclear vesicles labeled by antibody to CgA or CgB were deformed and fused together (**Fig. 2b**), possibly reflecting damage to the Golgi apparatus[31]. We also detected partial colocalization of mutant SOD1 with CgA and CgB in irregular and large vesicular structures of spinal neurons from *G37R SOD1* transgenic mice (**Fig. 2c**). In the *SOD1* (wild-type) transgenic mice, the distribution patterns of CgA and CgB were similar to those of nontransgenic mice with no obvious colocalization between wild-type SOD1 and chromogranins (**Fig. 2d**).

To confirm the distribution of mutant SOD1 in the endoplasmic reticulum (ER)-Golgi system, we carried out subcellular fractionation of spinal cord lysates from transgenic mice expressing wild-type SOD1 or G37R SOD1 at different ages. Western blot analysis clearly demonstrated that mutant SOD1 was recovered in both heavy and light membrane fractions containing mitochondria and microsomes (**Fig. 3a**). The calculation from the densitometric value of SOD1 monomer revealed that, in the preclinical stage (6 months old), 23.6% of G37R SOD1 was found in heavy membrane fractions, and 4.2% in light membrane fractions. For wild-type SOD1, 13.4% was found in heavy membrane fractions and 1.91% in light membrane fractions. After paralysis, 6.46% of monomeric G37R SOD1 accumulated in the light membrane

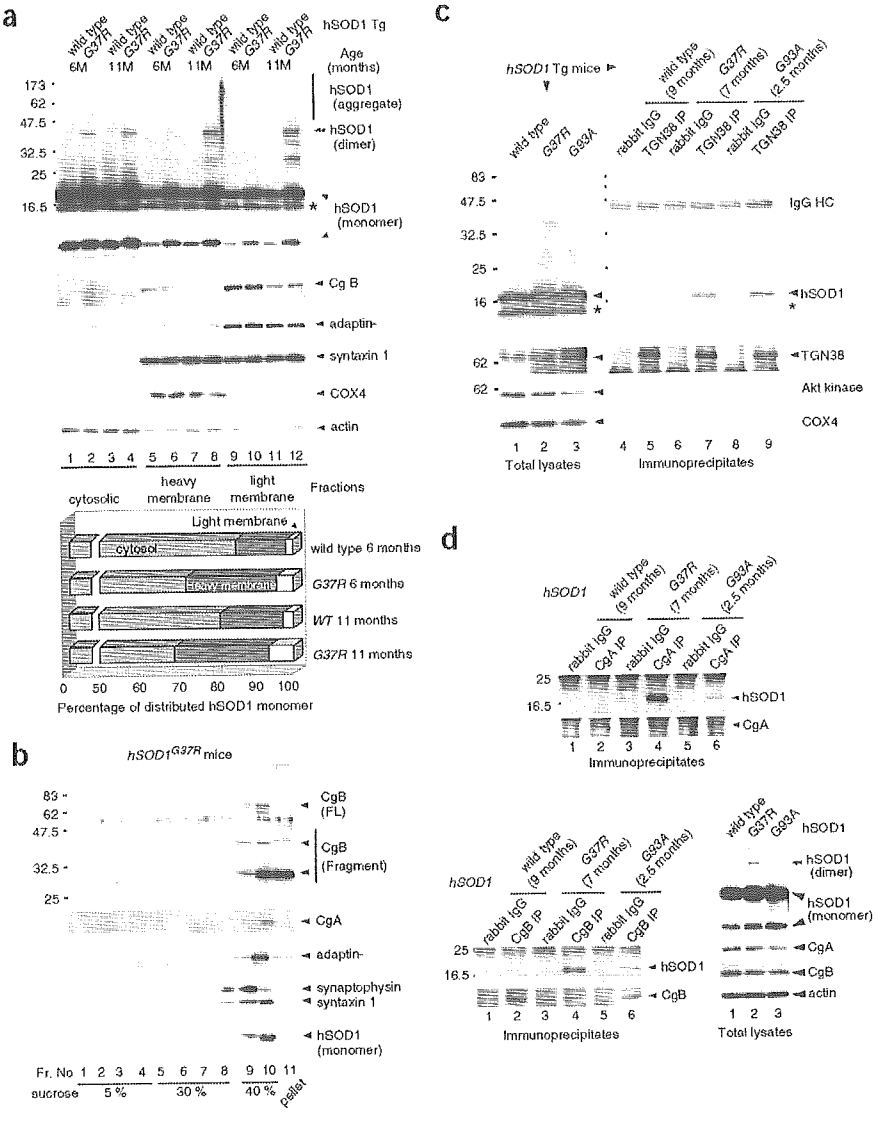

Figure 3 SOD1 mutants in spinal cord of ALS mice accumulate in TGN and co-immunoprecipitate with chromogranins. (**a**) G37R SOD1 accumulated in both heavy and light membrane fractions. Subcellularly fractionated proteins from spinal cord of wild-type and G37R *SOD1* transgenic mice (6 and 11 months old) was analyzed by western blotting using antibodies specific to human SOD1, CgB, adaptin-γ, syntaxin-1, COX4 and actin. Asterisk indicates endogenous mouse SOD1. The percentage of monomeric human SOD1 in each fraction was presented from the densitometric value of monomeric SOD1 in the cytosolic, heavy and light membrane fractions that was standardized by actin, COX4 and syntaxin-1, respectively (bottom). (**b**) Fractionation of microsome components by sucrose density-gradient ultracentrifugation showing that G37R SOD1 co-distributed with CgA, CgB, adaptin-γ and syntaxin-1. The light membrane fraction from spinal cord of G37R *SOD1* transgenic mice (7 months old) was analyzed. (**c**) Distribution of SOD1 mutants in the TGN. The spinal cord lysates from transgenic mice expressing human wild-type *SOD1* (9 months), G37R (7 months) or G93A (3 months) *SOD1* were immunoprecipitated with rabbit polyclonal anti-TGN38 preincubated with Protein G magnetic beads. The total tissue lysates and immunoprecipitates were analyzed by western blotting with antibodies to human SOD1, TGN38, Akt kinase and COX4. (**d**) Pull-down assay showing that CgA and CgB interacted with mutant SOD1 but not wild-type SOD1 in human SOD1 transgenic mice (wild-type, G37R and G93A). Spinal cord lysates were immunoprecipitated with anti-CgA or anti-CgB, which was analyzed using antibody to human SOD1.

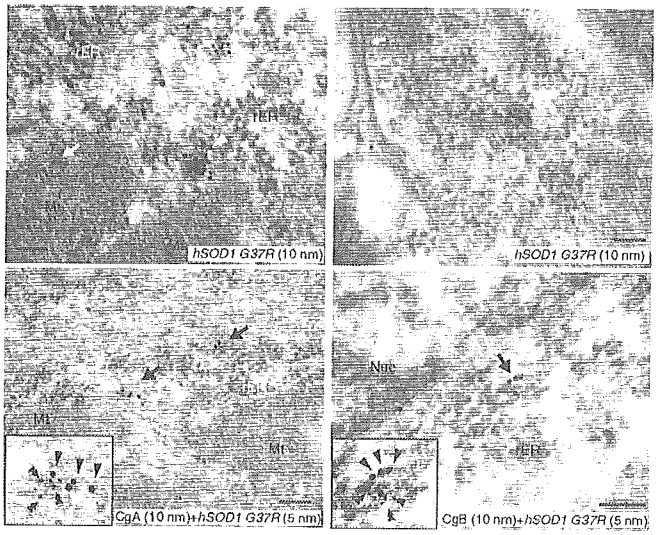

Figure 4 Immunoelectron microscopy reveals partial colocalization of G37R SOD1 with chromogranins. Ultra-thin sections of spinal anterior horn from G37R *SOD1* mice (7 months old) were incubated with sheep polyclonal antibody to human SOD1 alone (top panels), or together with rabbit polyclonal antibody to CgA or CgB (lower left or right, respectively). For secondary antibody, we used 10-nm (top panels) or 5-nm (bottom panels) immunogold-conjugated anti-sheep IgG and 10-nm immunogold-conjugated anti-rabbit IgG antibodies. In rough ER, 10-nm clusters of immuno-gold particles were frequently detected (arrowheads). G37R SOD1 was occasionally detected in mitochondria (arrow, top-left), or in a vesicle (arrowhead, top-right) close to the plasma membrane (arrows, top-right). Double-staining revealed frequent 10-nm clusters of CgA or CgB (arrowheads, bottom left or right) and 5-nm gold particles (hSOD1, double arrowheads, bottom panels). Scale bars, 100 nm.

fractions, whereas only 2.61% of wild-type SOD1 accumulated there (**Fig. 3a**, bottom). Furthermore, G37R SOD1 but not wild-type SOD1 formed non-native dimers and high molecular aggregates in the membrane fractions in an age-dependent manner. To further clarify the distribution of mutant SOD1 in the transport vesicles, we performed sucrose density gradient ultracentrifugation of post-mitochondrial membrane fractions using spinal cord extract from presymptomatic G37R *SOD1* transgenic mice at 7 months old. Western blotting revealed that mutant SOD1 had a distribution pattern similar to chromogranins, the trans-Golgi marker adaptin-γ and the SNARE protein syntaxin-1, but different from the pattern of synaptophysin (**Fig. 3b**).

To further confirm the distribution of mutant SOD1 species in a secretory pathway, we purified TGN from the spinal cord lysates of *SOD1* (wild-type), G37R *SOD1* and G93A *SOD1* transgenic mice by an immuno-isolation technique using anti-TGN38 antibody bound to protein G–coated magnetic beads. Anti-TGN38 is an affinity-purified polyclonal antibody specific to a 23-amino acid peptide corresponding to the cytosolic domain of rat and mouse TGN38 protein. Western analysis of the immunoprecipitates demonstrated that both G37R and G93A SOD1 co-precipitated with TGN38, indicating that mutant SOD1 is distributed in the TGN (**Fig. 3c**). Note that the wild-type SOD1 was also detectable in the TGN preparation, albeit at lower levels than mutant SOD1.

Further evidence for the specific interaction of CgA or CgB with mutant SOD1 proteins came from co-immunoprecipitation experiments using spinal cord lysates of transgenic mice. We found that rabbit polyclonal anti-CgA or anti-CgB antibody was able to pull down both G37R and G93A SOD1 mutants but not wild-type SOD1 (**Fig. 3d**). It should be noted that a non-native dimer of G37R SOD1 was more apparent than G93A SOD1 (double arrowhead), corresponding to the larger amount of co-immunoprecipitated G37R SOD1 than G93A SOD1.

To further investigate the distribution and colocalization of mutant SOD1 and chromogranins, we examined spinal cord sections from *SOD1* (wild-type) and G37R *SOD1* transgenic mice (7 months old) using immunoelectron microscopy. Mutant SOD1 protein was observed as small clusters of gold particles in the cytosol (**Supplementary Fig. 3** online), rough ER (arrowheads in **Fig. 4**, top-left), smooth ER and Golgi (**Supplementary Fig. 3**), and occasionally it was observed in mitochondria (arrow in **Fig. 4**, top-left) and transport vesicles (**Fig. 4**, top-right). Moreover, the double immunohistochemistry using secondary antibodies conjugated with different gold particles (5 nm or 10 nm) provided frequent detection of cluster complexes

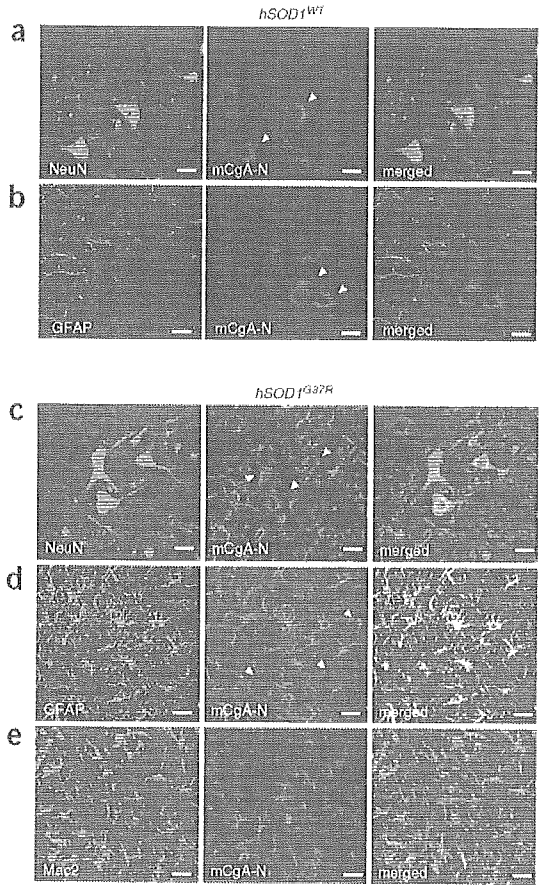

Figure 5 CgA is expressed in reactive astrocytes of spinal anterior horn from mutant *SOD1* transgenic mice. Double immunofluorescent experiments show the colocalization of CgA and GFAP in the spinal cord of transgenic mice carrying mutant *SOD1*, but not those carrying wild-type *SOD1*. (**a**,**b**) In wild-type *SOD1* mice, CgA was expressed only in the neurons labeled by anti-NeuN (**a**, mouse monoclonal), but not in reactive astrocytes labeled by anti-GFAP (**b**, mouse monoclonal). In G37R *SOD1* mice, in addition to the neuronal expression (**c**), CgA was also detected in reactive astrocytes (**d**), but not in the active microglial cells labeled by anti-Mac2 (**e**, rat monoclonal). Arrowheads and arrows, respectively, indicate neurons and astrocytes stained with anti-mCgA-N′. Left panels represent merged images from left and middle panels. Scale bars, 50 μm. Images show a representative sample from one of at least three independent experiments.